



## D1.1

# System scenarios and requirements specifications

<b>Project number:</b>	619086
<b>Project acronym:</b>	MAMMOET
<b>Project title:</b>	Massive MIMO for Efficient Transmission
<b>Project Start Date:</b>	1 January, 2014
<b>Duration:</b>	36 months
<b>Programme:</b>	FP7/2007-2013
<b>Deliverable Type:</b>	Report
<b>Reference Number:</b>	ICT-619086-D1.1
<b>Workpackage:</b>	WP 1
<b>Due Date:</b>	31 December, 2014
<b>Actual Submission Date:</b>	13 January, 2015
<b>Responsible Organisation:</b>	EAB
<b>Editor:</b>	Eleftherios Karipidis
<b>Dissemination Level:</b>	PU
<b>Revision:</b>	1.00
<b>Abstract:</b>	Key 5G mobile broadband scenarios, for which massive MIMO is mostly relevant, are described. The envisioned operation of a massive MIMO system is outlined, focusing on PHY technical functionality. The total BS power consumption is modeled. The main performance metrics of spectral and energy efficiency are elaborated. Several tradeoffs are discussed.
<b>Keywords:</b>	5G, MBB, scenarios, massive MIMO, power consumption, spectral efficiency, energy efficiency, hardware impairments



This project has received funding from the European Union's Seventh Framework Programme for research, technological development and demonstration under grant agreement no. 619086.

## **Editor**

Eleftherios Karipidis(EAB)

## **Contributors (ordered according to beneficiary numbers)**

Christina Petschnigg (TEC)

Naeim Safari (TEC)

Claude Desset (imec)

Liesbet Van der Perre (imec)

Eleftherios Karipidis (EAB)

Franz Dielacher (IFAT)

Ioannis Papananos (IFAT)

Ibrahim Kazi (KUL)

Wim Dehaene (KUL)

Fredrik Tufvesson (ULUND)

Emil Björnson (LiU)

Hei Victor Cheng (LiU)

Erik G. Larsson (LiU)

Daniel Persson (LiU)

Javier Lorca Hernando (TID)

## Executive Summary

MAMMOET aims to bring massive MIMO from an initial promising concept to a highly attractive technology for usage in future broadband mobile networks. In order to achieve this goal, the project has a number of important scientific and industrial objectives, one of which is to elaborate system concepts and approaches. This deliverable sets the scene for the work in MAMMOET by specifying the system outline and scenarios, defining the relevant performance metrics, identifying fundamental limits, and addressing trade-offs for practical implementation.

The massive MIMO concept can only be understood and described properly if appropriate system scenarios are envisaged, with the goal of enabling actual capacity and energy improvements. A minimum set of diverse and challenging 5G mobile broadband scenarios that are mostly relevant to massive MIMO are presented in Chapter 1. Scenarios definitions amount on specifying the values of a set of parameters that are common to all scenarios and elaborating the main characteristics that are specific to each scenario. The selection of the prioritized scenarios has been driven by both technical and business related criteria. This ensures that MAMMOET results focus on demonstrating substantial capacity and energy gains while maximizing the potential impact, targeting to increase the chances for adoption in commercial exploitation. Moreover, the baseline scenarios for performance comparisons are identified.

The massive MIMO concept considered in MAMMOET is envisioned to be a key technical feature of 5G systems, targeting to increase the spectral efficiency by orders of magnitude over contemporary systems. It relies on equipping BSs with hundreds or thousands of antenna elements which, unlike conventional cellular technology, are operated in a phase-coherent fashion. This can provide unprecedented array gains and a spatial resolution that allows for multi-user MIMO communication to tens or hundreds of UEs per cell, while maintaining robustness to inter-user interference. The main operation of massive MIMO is outlined in Chapter 2 focusing on physical layer technical functionality. The uplink and downlink signaling are defined in a TDD-based transmission protocol and pilot-based channel estimation in the uplink is described. The average spectral efficiencies achieved in such a system with a diverse selection of linear precoding/combining schemes are derived.

In order to properly evaluate massive MIMO solutions, it is important to model apart from the achievable throughput at different system levels (per user, cell, and area), the corresponding power consumption. Given the fundamental differences between massive MIMO BSs and traditional (macro) BSs, estimating their power consumption requires a significant modeling effort, taking into account all the different components in order to assess the total system power consumption. This is achieved in Chapter 3 to accurately define the energy efficiency metric. Along the way, the innovative transmitter architecture developed in MAMMOET is highlighted.

The spectral efficiencies achieved by massive MIMO in a variety of different setups are illustrated in Chapter 4. An asymptotic analysis is first given and then complemented by simulation results of optimized performance evaluations. The effect of the main scenario parameters and the impact of hardware impairments are investigated. Moreover, scaling behaviors and practical trade-offs are discussed. These results provide fundamental limits of the massive MIMO performance and the conclusions yield a valuable first insight that will be used to steer the MAMMOET research on algorithm development around the topics of channel estimation, pilot allocation, and phase-coherent precoding/combining.

The system approach of massive MIMO is concluded with a consideration of physical layer security. A preliminary analysis of the main security approaches is reported in Chapter 5, with emphasis on the power approach. Open issues for practical applicability of these approaches in massive MIMO systems are identified.

# Contents

<b>1</b>	<b>5G mobile broadband scenarios relevant to massive MIMO</b>	<b>1</b>
1.1	Scenarios principles . . . . .	2
1.1.1	Scenarios scope . . . . .	3
1.1.2	Scenarios prioritization . . . . .	4
1.1.3	Relation to METIS . . . . .	4
1.2	Common scenarios parameters . . . . .	5
1.3	Main characteristics of massive MIMO scenarios . . . . .	8
1.3.1	Scenario 1: Open exhibition . . . . .	8
1.3.2	Scenario 2: Massive connectivity with crowded buildings . . . . .	9
1.3.3	Scenario 3: Ubiquitous connectivity for the urban society beyond 2020 . . . . .	9
1.3.4	Scenario 4: Crowded auditorium . . . . .	10
1.3.5	Scenario 5: Wide area with mobility . . . . .	12
1.4	Baseline scenarios . . . . .	13
1.4.1	Outdoor - 3GPP LTE Rel. 8 . . . . .	13
1.4.2	Indoor - IEEE 802.11ac . . . . .	14
<b>2</b>	<b>Massive MIMO system outline</b>	<b>18</b>
2.1	Basic concept and transmission protocol . . . . .	18
2.2	Uplink signaling . . . . .	19
2.3	Downlink signaling . . . . .	20
2.4	Pilot-based channel estimation . . . . .	20
2.5	Average achievable spectral efficiencies . . . . .	22
<b>3</b>	<b>Performance metrics</b>	<b>25</b>
3.1	Modeling of total power in massive MIMO systems . . . . .	25
3.1.1	Power amplifier . . . . .	26
3.1.2	Analog front-end . . . . .	26
3.1.3	Digital baseband . . . . .	27
3.1.4	Power system . . . . .	28
3.1.5	Current estimates and further developments . . . . .	28
3.1.6	Alternative transmitter architecture . . . . .	29
3.2	Definition of performance metrics . . . . .	31
<b>4</b>	<b>Performance analysis, fundamental limits, and tradeoffs</b>	<b>32</b>
4.1	Asymptotic analysis . . . . .	32
4.2	Optimizing performance in hexagonal networks . . . . .	33
4.2.1	Optimizing spectral efficiency for different interference levels . . . . .	34
4.2.2	Impact of scenario parameters . . . . .	37
4.3	Impact of hardware impairments . . . . .	39



4.4	Specific scaling behaviors and trade-offs . . . . .	41
4.4.1	Energy efficiency tradeoffs . . . . .	42
4.4.2	Power allocation for realistic amplifier models . . . . .	42
4.4.3	Operation of massive MIMO in low traffic scenarios . . . . .	43
<b>5</b>	<b>Physical layer security for massive MIMO</b>	<b>46</b>
5.1	Background on physical layer security . . . . .	46
5.2	Classification techniques . . . . .	46
5.2.1	Power approach . . . . .	46
5.2.2	Coding approach . . . . .	48
5.2.3	Channel approach . . . . .	48
5.3	Open issues . . . . .	49

# List of Figures

1.1	“Great service in a crowd” scenario from METIS D1.1 [1]. . . . .	4
1.2	Possible antenna configurations and deployment scenarios for a massive MIMO BS. . . . .	7
1.3	Madrid grid for evaluations of METIS TC2 [1]. . . . .	11
1.4	Scenarios and usage models under consideration in IEEE HEW SG [4]. . . . .	15
1.5	Illustration of a real-world scenario for IEEE 802.11ac evaluations [4]. . . . .	16
1.6	Proposal of scenario parameters under consideration in IEEE HEW SG [4]. . . . .	17
2.1	The transmission is divided into frames of $S = T_c W_c$ symbols, whereof $B$ symbols are dedicated to pilots. The remaining $S - B$ symbols are used for payload data, where $\zeta^{(\text{ul})}$ and $\zeta^{(\text{dl})}$ are respectively the fractions of UL and DL transmission. . . . .	19
3.1	“Conventional” transmitter (with DFE+DAC+mixer+LO+PGA+Driver+SAWs). . . . .	29
3.2	Digital RF modulator on a chip. . . . .	30
4.1	Part of a hexagonal network, colored for different pilot reuse factors $\beta$ . . . . .	33
4.2	Simulation of optimized SE, as a function of $M$ , with average inter-cell interference. . . . .	34
4.3	Simulation of optimized SE, as a function of $M$ , with best-case inter-cell interference. . . . .	35
4.4	Simulation of optimized SE, as a function of $M$ , with worst-case inter-cell interference. . . . .	36
4.5	Impact of changing the pilot reuse factor $\beta$ , for a system optimized for high per-cell SE. . . . .	38
4.6	Achievable SE per UE, for a system optimized for high per-cell SE. . . . .	38
4.7	Number of BS antennas per UE, for a system optimized for high per-cell SE. . . . .	39
4.8	Achievable per-cell SE as a function of the number of scheduled UEs. . . . .	39
4.9	Impact of SNR variations on the SE. . . . .	40
4.10	Impact of pathloss variations on the SE. . . . .	40
4.11	Per-cell SE as a function of the coherence block length $S$ . . . . .	41
4.12	Optimized per-cell SE with or without hardware impairments. . . . .	42
4.13	Number of BS antennas in use against fraction of maximum rate, when operating at low SNR. . . . .	44
4.14	Number of BS antennas in use against fraction of maximum rate, when operating at moderate SNR. . . . .	45
4.15	Number of BS antennas in use against fraction of maximum rate, when operating at high SNR. . . . .	45
5.1	Secret communication model [50]. . . . .	47
5.2	MIMO interference model [44]. . . . .	48

# List of Tables

1.1	Main requirements and KPIs from METIS D1.1 [1]. . . . .	5
1.2	Common parameters for the proposed massive MIMO scenarios. . . . .	6
1.3	“Open exhibition” main characteristics. . . . .	8
1.4	“Massive connectivity with crowded buildings” main characteristics. . . . .	9
1.5	“Ubiquitous connectivity for the urban society beyond 2020” main characteristics. . . . .	10
1.6	“Crowded auditorium” main characteristics. . . . .	12
1.7	“Wide area with mobility” main characteristics. . . . .	12
1.8	Minimum coupling losses (MCL) [47]. . . . .	13
3.1	Reference power consumption of analog sub-components (2012). . . . .	27
3.2	Power consumption: conventional and digital transmitter solutions. . . . .	30

# Chapter 1

## 5G mobile broadband scenarios relevant to massive MIMO

The massive multiple-input multiple-output (MIMO) concept (outlined in Chapter 2) can only be understood and described properly if appropriate system scenarios are envisaged, with the goal of enabling actual capacity and energy improvements.

New challenges are emerging for future 5G and pre-5G systems, among them:

- High user densities and required service traffic are expected in venues, shopping malls, stadiums, conferences, sports events, etc. These “crowded” situations pose a lot of capacity challenges for current network deployments based on small cells or Wi-Fi access points, being one of the issues the demand for a high-capacity backhaul network;
- The extreme expected densification of access points, both indoors and outdoors, is likely to end up with significant inter-cell interference that ultimately limits performance.

The above challenges share the property of advancing a huge concentration of active users in a reduced area. One typical example is a centre city square (such as, e.g., New York’s Times Square), especially during significant events (such as, e.g., New Year’s Eve).

Massive MIMO represents a major breakthrough in multi-antenna research that could pave the way for an efficient solution to such scenarios, offering drastically higher capacity, at much better energy efficiency. At least three major improvements are expected from massive MIMO systems that deserve special attention:

- Channel characteristics are improved with respect to current MIMO systems employing only few antennas. Some of the operational issues in MIMO can thus be avoided (such as insufficient number of eigen-modes, degeneracy of the channel with line-of-sight (LOS) conditions, etc.);
- The effects of hardware impairments can be averaged out and appear as additional white noise, thereby relaxing the radio frequency (RF) requirements at the base station (BS);
- The additional degrees of freedom provided by the antennas in excess can be used for waveform tailoring so as to reduce the peak-to-average power ratio (PAPR) of the radiated signal.

For these improvements to be observed in real systems, it is essential to identify which mobile broadband scenarios are most in need of the benefits offered by massive MIMO. This is accomplished in the rest of this chapter.

## 1.1 Scenarios principles

A minimum set of system scenarios are defined with the intention to:

- Represent commonly agreed network environments where current technologies are not sufficient to address (future) service requirements and where advantages are likely to be observed by the introduction of massive MIMO;
- Constitute network scenarios with a sufficiently attractive business case and/or exploitation plan for operators;
- Lead to a common framework for performance evaluations in MAMMOET, either by means of simulations or by direct measurements from the LuMaMi testbed [3]; and
- Steer channel measurement campaigns towards the most relevant network scenarios, yielding appropriate channel models to be used within the project.

The initial ambition level is to specify diverse and challenging scenarios that on the one hand span the problem space, but on the other hand lead to a limited number (e.g., not more than a handful) of representative use cases. A subset of those use cases will be eventually analysed thoroughly in MAMMOET, by means of simulations and/or testbed demonstrations and measurements. Inevitably, not all scenarios can be quantitatively analysed in the context of a small-scale project such as MAMMOET, because of limited simulation capabilities and/or constrained testbed hardware, but this does not mean that they are of no interest. On the contrary, the intention of this document is to reflect the most representative scenarios, even if they cannot be completely analysed within the project, thus paving the way for further research and development, and eventually deployment of massive MIMO technology on a broader scale. In addition, not all the details of the scenarios can be provided from the beginning in a closed and static form. The goal is rather to highlight the main characteristics and key parameters of the most representative scenarios and avoid the risk of over-specification. The deliverable has the intention to be a *living* document; that is, the scenarios descriptions in this chapter will be complemented, updated, and refined throughout the life of the project.

The purpose of having several scenarios is to break down an initially complex problem into smaller sub-problems, so that not all the characteristics of a realistic network setup are analysed at once. Each of the scenarios addresses a specific issue to be analysed, while simplifying other assumptions even if it may result in an unrealistic situation. The most important differentiator of the scenarios is the propagation environment, being either outdoor, outdoor-to-indoor, or indoor. Still there is one specific case where the consortium has decided to keep several of the main characteristics at once, thus resembling a typical dense urban layout more closely. However, in this latter case the ambition level for analysis may have to be somewhat lowered if complexity results in too much processing time for the simulations.

The agreed baseline reference that will be used for comparison of the relative performance gains depends on the type of propagation environment considered:

- For outdoor scenarios it will be LTE Release 8, operating in time-division duplex (TDD) mode, with 3GPP urban macro (UMa) channel model and two independent streams, as a representative of the most relevant technology encountered in practice outdoors.
- For indoor scenarios it will be IEEE 802.11ac, as a representative of the most typical high capacity technology found indoors.

It is clear that more advanced technologies could be considered as a reference, e.g. LTE Release 12 for outdoors. However its interest as a reference is much more limited given that it was standardised only recently and no practical deployments and/or experiences have been found so far. In addition, performance above LTE Release 8 usually relies on the assumption of having multiple receive antennas at the user equipment (UE) (up to 8 for maximum capacity) and increased system bandwidths (up to 100 MHz), both assumptions being yet hardly achievable in practice. Therefore, LTE baseline system with 20 MHz system bandwidth and up to two receive antennas at the UE is considered to be much more representative of current state-of-the-art.

### 1.1.1 Scenarios scope

Generally speaking, the scope of the defined scenarios has followed two paths, which together address the most stringent capacity-requiring use cases:

- Outdoor situations comprising a massive MIMO cellular setup, with a given (in principle large) number of antennas concentrated at the BS. These scenarios represent the main body of interest as they can potentially show higher advantages compared to traditional cellular setups in very crowded situations. Even if the BS is to be located outdoors, users may be both indoors or outdoors, thus giving rise to interesting cases with either purely outdoor or mixed outdoor-to-indoor propagation conditions.
- Indoor situations where both the massive MIMO BS and the users are located indoors. This case is traditionally covered by indoor wireless solutions like Wi-Fi, which suffer from a number of drawbacks that may be (partially) overcome by massive MIMO solutions.

Inter-cell interference with very dense deployments can be significant in both cases. Techniques based on inter-cell interference coordination would therefore be required to avoid significant performance degradation at the boundaries between cells. These techniques are however out of the scope of the project, thus focusing ourselves to the transmission and reception procedures and associated performance metrics. Further studies should elaborate on effective solutions to keep inter-cell interference under certain limits (especially outdoors).

In all cases, concentrated BSs (with multiple antennas at the same site) are considered, as being the most realistic case because of technical and practical reasons. Distributed BSs (comprising multiple remote radio heads fibre-connected to the baseband processing unit) are out of the scope due to several reasons:

- Complexity in performing centralised baseband processing in real time.
- Difficulty in characterising the propagation environment. Results will probably be highly dependent on the actual arrangement of the distributed antenna elements, and only a few channel measurements are available so far for such antenna configurations; see [22] and the references therein.
- Costly fronthaul network connecting the remote radio heads to the central baseband unit. Fronthaul fibre links would require huge capacities for the transport of digitized in-phase quadrature (IQ) signals (approximately 1.2 Gbps required for LTE 20 MHz with common public radio interface), leading to very costly operation and maintenance.

Note that centralization only concerns the BS equipment, as users will be, by definition, distributed throughout in all scenarios.

Finally, the users are assumed to have one or two receive antennas (mainly for increased diversity, but single-user (SU)-MIMO is not precluded) and only one transmit antenna. Receive processing at the UE side will be based on standard single-user techniques whenever possible, by performing all massive MIMO-related processing at the BS.

### 1.1.2 Scenarios prioritization

Priorities will also be provided along with the use cases description. Priorities are a straightforward way to restrict the scope and the number of possible scenarios, but in practice the prioritization exercise can be a complex one due to several factors influencing it:

- **Business relevance** – are the most prioritized scenarios also the most interesting ones in terms of business case?
- **Technical challenge** – are scenarios focused on challenging network deployments for which standard solutions have proven to be inadequate?
- **Potential to achieve gains over state-of-the-art** – are scenarios focusing on those situations with higher chances to show larger gains?
- **Feasibility of channel measurements, testbed demonstrations and/or simulations** – are scenarios focusing only on those ones for which simulations/measurements are available?

In this project we have made an initial prioritization exercise that combines all the above factors, thus yielding an ordered list that takes into account business factors, technical factors and performance evaluation factors altogether. Further versions of this deliverable will refine the agreed scenarios in a continuous way throughout the project.

### 1.1.3 Relation to METIS

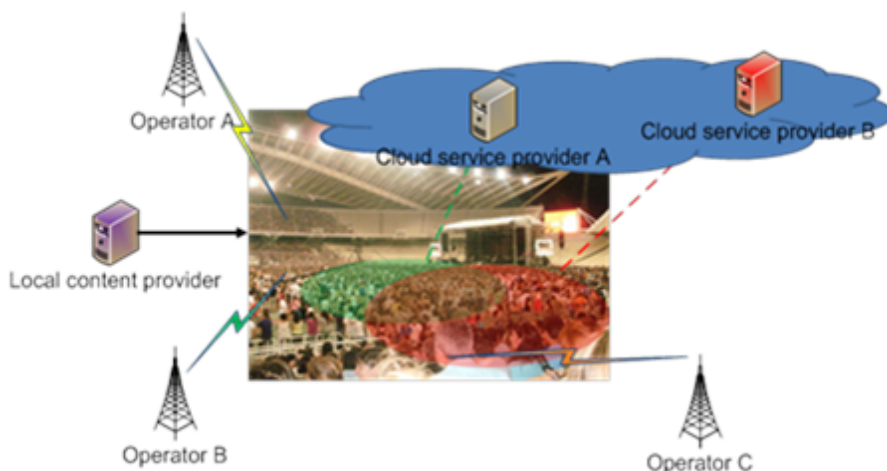


Figure 1.1: “Great service in a crowd” scenario from METIS D1.1 [1].

The scenarios to be described are selected so as to complement the definition of 5G mobile broadband scenarios by EU FP7 METIS project [1]. The focus is on identifying and elaborating the scenarios which are most relevant to massive MIMO. One of METIS scenarios (namely

“Great service in a crowd”) specifically addresses the end-user demands for future communication solutions to work well in a crowd (Figure 1.1). The main technical difficulty in this scenario to be faced by future cellular communication systems is the ability to provide great service to a very dense crowd of users.

A number of test cases (TC) were further defined in METIS so as to assess whether each of the proposed technical solutions could fulfil the challenges of each scenario. Among them, the TCs with the highest relevance to massive MIMO are collected and summarized in Table 1.1 [1]. For each TC, the main 5G requirements are listed for the key performance indicators (KPIs) of relevance to MAMMOET.

Table 1.1: Main requirements and KPIs from METIS D1.1 [1].

METIS Test Case	MAMMOET-relevant KPIs	5G Requirements
TC1 “Virtual reality office”	Traffic volume density	Average 100 Mbps/m <sup>2</sup> in both DL and UL; peaks can be 5 times higher
	Experienced user throughput	At least 1 (5) Gbps DL+UL with 95% (20%) availability
TC2 “Dense urban information society”	Traffic volume density	About 700 Gbps/km <sup>2</sup> DL+UL
	Experienced user throughput	300 (60) Mbps in DL (UL) with 95% availability
TC3 “Shopping mall”	Traffic volume density (during shopping busy period –hour–)	About 170 (67) Gbps/km <sup>2</sup> in DL (UL)
	Experienced user throughput	Intermediate data rates for bursty traffic pattern of at least 300 (60) Mbps in DL (UL)
TC4 “Stadium”	Traffic volume density	0.1-10 Mbps/m <sup>2</sup> (stadium area 50,000 m <sup>2</sup> )
	Experienced user throughput	0.3-20 Mbps DL+UL
TC9 “Open air festival”	Traffic volume density	900 Gbps/km <sup>2</sup> DL+UL
	Experienced user throughput	Over 30 Mbps during busy period (DL/UL) at 95% availability

## 1.2 Common scenarios parameters

Some common parameters can be identified for all scenarios under study from a high-level perspective. Table 1.2 collects the values of these parameters according to the RF and baseband requirements agreed by the consortium for the simulations and/or demonstrations. Even if in practice not all the common parameters collected in Table 1.2 may have the same values for the scenarios described next in Section 1.3, we intentionally restrict their values to be similar for all the cases in order to align the simulations and part of the testbed configuration to a common set of assumptions. This is important especially regarding the hardware involved, as it cannot usually be changed regarding the operating frequency, number of antennas, etc.

Common assumptions behind these parameters are given in the following list.

Table 1.2: Common parameters for the proposed massive MIMO scenarios.

Parameter	Value
Operational frequency	3.7 GHz
Bandwidth	20 MHz
BS antennas	100 (up to 128 for LuMaMi)
BS antenna configuration	Rectangular array, $\lambda/2$ separation, dual polarization
UE antennas	1 TX antenna; 1 or 2 RX antennas
BS antenna gain	7-9 dB corresponding to patch antenna
UE antenna gain	0 dB
Total BS output power	Up to 46 dBm
Per-antenna output power	10 dBm average; up to about 16 dBm peak
UE output power	Up to 27 dBm (limited to 16 dBm in LuMaMi)
BS noise figure	5-7 dB
UE noise figure	5-7 dB
Baseline technology	OFDM, TDD
Max active UEs	10
Min modulation, coding rate	BPSK, 1/5
Max modulation, coding rate	64QAM, 5/6
User traffic pattern	Full buffer

- **Operating frequency.** In the project we will assume that cmWave frequencies are used below 6 GHz. Going above 6 GHz would require brand new channel models, as well as different types of signal impairments not covered by current channel models (like ITU COST2100, 3GPP SCME, etc.). In addition, RF hardware implementations for such higher frequencies is still not sufficiently mature, and may suffer from excessive phase noise or other impairments (while being significantly more costly).
- **User mobility** is initially considered not to be high, e.g. less than 30 km/h. However higher user speeds could be handled by massive MIMO and be reflected in some of the scenarios, the only limitation being the proper selection of the signal frame duration so as not to suffer from channel aging effects.
- **Interference from neighbour cells/systems** is considered to be additive white Gaussian noise (AWGN), thereby precluding more realistic effects which are characteristic of systems with multiple cells (either massive MIMO or based on traditional techniques). Although the effects of intra-cell channel impairments will be taken into account, as well as so-called pilot contamination effects (from the reuse of limited numbers of pilot sequences for uplink estimation), any other inter-cell interference effects will be averaged out as AWGN.
- **The number of antennas at the UE** will be one or two, the latter being used for increased diversity (to improve the receive SINR), but dual-stream SU-MIMO can also be further incorporated to the overall multiuser (MU)-MIMO concept to increase individual peak rates.
- **The system bandwidth** will be 20 MHz because of the relatively lower frequencies considered (below 6 GHz), for which availability of larger chunks of spectrum is problematic. Further, beyond MAMMOET, research on massive MIMO for mmWave bands could avoid this assumption and consider much wider system bandwidths.

- **The target spectral efficiency** for the users will be roughly 1 bps/Hz, with the objective of achieving uniform user experience throughout the cell (as opposed to large peak data rates at the cell centre at the cost of very poor behaviour at the cell edge). This target may be increased if SU-MIMO is finally incorporated in the simulations with two receive antennas, or if beamforming techniques can complement MU-MIMO spatial multiplexing to overcome poor coverage conditions. Given that users could be granted the whole system bandwidth, large data rates would in principle be possible for all users even with a modest spectral efficiency target.
- **Massive antenna array is concentrated** at the BS, thus avoiding distributed array configurations. Planar arrays with half-wavelength separation between antenna elements will be considered. Other array geometries (e.g. linear, cylindrical...) can be employed for other purposes (e.g. to measure massive MIMO channel characteristics [28]), but generally a planar array will be considered due to its ease of implementation and similarity with current MIMO antenna arrangements. The final number of antenna elements will depend on the scenario under consideration. Figure 1.2 illustrates possible antenna arrangements (both concentrated and distributed) that could both be possible conceptually, while the concentrated scenario is to be expected mostly in potential practical deployments.

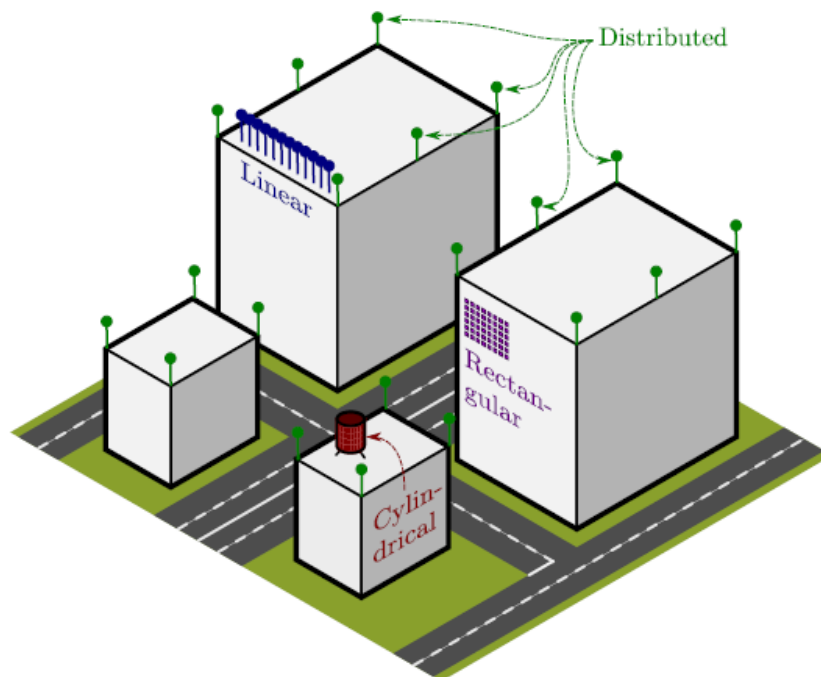


Figure 1.2: Possible antenna configurations and deployment scenarios for a massive MIMO BS.

- Duplexing mode will be TDD, because of significant concerns on the feasibility to report channel feedback between each user and each of the massive MIMO antennas in frequency-division duplex (FDD) systems.
- Traffic pattern of users will be similar in all scenarios, and selected as the one showing more relevance for massive MIMO (e.g. video streaming or even full-buffer traffic). Actual selection of user traffic patterns is left for further analysis throughout the project, according to the simulation capabilities and the type of tests to be run in the hardware

demonstrator. Thanks to the TDD duplex mode the uplink (UL) and downlink (DL) traffic patterns can be made either symmetrical or asymmetrical. However, for simplicity and unless otherwise noted, the project will consider mainly symmetrical UL/DL traffic configurations.

## 1.3 Main characteristics of massive MIMO scenarios

In this section, we present the main characteristics of the massive MIMO scenarios, in the order that they have been prioritized by the consortium.

### 1.3.1 Scenario 1: Open exhibition

This scenario comprises of outdoor-deployed (macro) BSs serving outdoor-located UEs. UEs with high density are randomly distributed and moving at pedestrian speeds. UEs locations are in principle completely random, although some correlation may exist for both the UEs positions and the traffic patterns at specific times and/or locations. Extreme-capacity service is provided in medium to large, depending on the transmit power, outdoor areas with delimited geometry, e.g., by the boundaries of an outdoor conference center. In such propagation environments, the channels can in principle have both LOS and NLOS components. This scenario has been the natural starting point for the massive MIMO channel measurement campaigns, currently ongoing in the context of MAMMOET WP1, due to the relatively straightforward setup.

Due to the relatively low propagation loss, this scenario has high potential to demonstrate the capacity advantages of massive MIMO. Current state-of-art solutions based on WiFi or small cells suffer from a number of drawbacks that demand more effective solutions, being among them the difficulties in achieving real coordination of resources among the nodes, and the cost of a proper backhaul network (both wired or wireless) able to cope with the expected amount of traffic during busy times.

Examples of such scenario are outdoor conference centers and crowded squares. This scenario relates with METIS TC9 “open air festival” on the propagation environment aspects, but not necessarily on the infrastructure limitations of TC9. The main characteristics of the “open exhibition” scenario are summarized in Table 1.3.

Table 1.3: “Open exhibition” main characteristics.

Parameter	Value
Propagation environment	Outdoor
Cell geometry / size	Irregular, delimited geometry / medium to large
UE distribution	Random, but clustered, with high density
UE speed	Up to 7 km/h
LOS/NLOS	Both
Shadow fading	Present
Channel model	COST2100
METIS relation	TC9 “Open air festival”
Examples	Outdoor conference center, crowded square

### 1.3.2 Scenario 2: Massive connectivity with crowded buildings

This scenario corresponds to a classical indoor environment where service is provided from an outdoor massive MIMO solution instead of an indoor specialised deployment. One of the major challenges that modern networks face is the deployment and service location mismatch. While macro BS are deployed outdoors, about 80 – 90% of current traffic comes from indoors [2], and this trend is likely to increase in the coming years with the pervasive presence of different devices (tablets, laptops etc.) with strong multimedia capabilities. In spite of the popularity of indoor solutions (such as distributed antenna systems (DAS), WiFi or pico cells), all of them suffer from significant issues in terms of cost and operational complexity. Massive MIMO represents an elegant solution, with apparent business relevance, that can potentially exploit both the horizontal, as well as the vertical dimensions to serve indoor users at different storeys.

This scenario could be split into two sub-cases: one dealing with low-rise buildings (e.g. shopping malls), where users can be considered to reside in roughly the same horizontal plane (from the viewpoint of the antennas), and another dealing with high-rise buildings (e.g. skyscrapers). The latter would likely involve special (so-called elevation) beamforming capabilities (in addition to MU-MIMO) and quantitative analysis requires accurate 3D channel models. The consortium decided to focus on the first sub-case, thus leveraging on MU-MIMO techniques.

In this scenario, the cell size is delimited by the building geometry and indoor furniture. The UEs are randomly distributed with high density and are almost static in most cases. NLOS propagation conditions are expected and the major technical challenge is to overcome the possibly high outdoor-to-indoor penetration loss, e.g. due to metalized windows. In such a case, high antenna directivity is not always a good strategy since most of the energy will be reflected somewhere else. However, high gain beamforming may be used to find and utilize beneficial multi-path like reflections in surrounding buildings or to direct the beam towards parts of the wall that have lower penetration loss.

Examples of such scenarios are office buildings, blocks of flats, shopping malls, and residential areas. This scenario relates with METIS TC3 “shopping mall”. The main characteristics of the “massive connectivity with crowded buildings” scenario are summarized in Table 1.4.

Table 1.4: “Massive connectivity with crowded buildings” main characteristics.

Parameter	Value
Propagation environment	Outdoor-to-indoor
Cell geometry / size	Determined by building sizes and geometries / a single BS can typically serve one building
UE distribution	Random, with high density
UE speed	Mostly static, up to 3 km/h, except in shopping mall
LOS/NLOS	NLOS
Shadow fading	Present
Channel model	COST 2100 extended with outdoor-to-indoor model
Examples	Office, block of flats, shopping mall, residential area
METIS relation	TC3 “Shopping mall”

### 1.3.3 Scenario 3: Ubiquitous connectivity for the urban society beyond 2020

This scenario represents the most ambitious case of providing, with an outdoor deployed network, uniform user experience in realistic ultra-dense urban environments, including both out-

door and indoor locations, with complex RF propagation conditions. It represents the most interesting case in terms of business opportunities for operators, where massive broadband wireless access is to be demanded everywhere, at all times. Random users (both outdoors and indoors) at speeds up to approximately 30 km/h can populate residential areas, shopping malls, or office buildings with a strong demand for data consumption. The scenario corresponds to a realistic city layout, with geometry delimited by buildings, streets and urban furniture. Similar to METIS TC2 “dense urban information society”, it represents a typical European city environment capturing way more aspects than the Manhattan grid. It may be considered as a combination of the simpler Scenarios 1 and 2 defined in Sections 1.3.1 and 1.3.2, respectively. The main characteristics of the “ubiquitous connectivity for the urban society beyond 2020” scenario are summarized in Table 1.5.

Table 1.5: “Ubiquitous connectivity for the urban society beyond 2020” main characteristics.

Parameter	Value
Propagation environment	Outdoor and outdoor-to-indoor
Cell geometry / size	Irregular, depending on urban layout / ultra-dense urban deployment with short inter-site distances
UE distribution	Random, with high density
UE speed	Up to 30 km/h
LOS/NLOS	Both
Shadow fading	Present
Channel model	COST 2100 extended with outdoor-to-indoor model
Examples	Realistic dense city with high density of users
METIS relation	TC2 “Dense urban information society”

Even though this scenario is labeled as the most ambitious, yet it has not been given the highest priority, as for high capacity this is not the most stringent. The main challenge of this scenario is to provide same quality of experience in diverse environments; MAMMOET envisions that massive MIMO will be a key component of the technical solution that will accomplish this. Moreover, this scenario is the most challenging to analyse quantitatively, as ray-tracing propagation and system-level simulations are required to assess the gains. This effort is beyond the scope and capabilities (in terms of resources) of MAMMOET. However, it is still an important scenario for MAMMOET, as the massive MIMO channel model being developed in WP1 will be relevant for a mixed outdoor and outdoor-to-indoor propagation environment. Finally, the consortium is currently considering the possibility to perform simulation studies in this scenario by exploiting synergies with METIS. Specifically, by using the publicly available<sup>1</sup> Madrid grid test layout shown in Figure 1.3 that has been used for massive MIMO evaluations in METIS TC2.

### 1.3.4 Scenario 4: Crowded auditorium

This scenario represents the indoor counterpart of the outdoor Scenario 1, defined in Section 1.3.1, in which both the UEs and BSs are, respectively, located and deployed indoors. The UEs are randomly distributed with high density, possibly with correlated UEs positions and traffic patterns. The UEs are almost static in most cases and NLOS propagation conditions are expected. A subcase may be considered in which the UEs are static, placed at deterministic locations (e.g., seats in a concert hall) and channels contain LOS components. The cell geometry

<sup>1</sup><https://www.metis2020.com/documents/simulations/>



interest for indoor deployments is mainly limited to corporate solutions, due to cost. The main characteristics of the “crowded auditorium” scenario are summarized in Table 1.6.

Table 1.6: “Crowded auditorium” main characteristics.

Parameter	Value
Propagation environment	Indoor
Cell geometry and size	Determined by scenario boundaries
UE distribution	Random, but clustered, with high density
UE speed	Mostly static, up to 3 km/h
LOS/NLOS	Both
Shadow fading	Not present
Channel model	COST2100
Examples	Indoor conference center, office, concert hall, indoor arena
METIS relation	TC1: “Virtual reality office”, TC3 “Shopping mall”, TC4: “Stadium”

### 1.3.5 Scenario 5: Wide area with mobility

This scenario represents an extension of the outdoor Scenario 1 in Section 1.3.1, mainly in the following two aspects. First, cell sizes are substantially larger, such as in suburban and rural areas, resulting to channels with longer delay spread. Second, higher mobility conditions (e.g., up to 70 km/h) are accommodated. These conditions lead to relatively shorter coherence intervals and pose challenging research questions that MAMMOET is addressing to demonstrate the efficiency of the massive MIMO concept in TDD mode.

Table 1.7: “Wide area with mobility” main characteristics.

Parameter	Value
Propagation environment	Outdoor
Cell geometry / size	Regular, wide area cells mainly delimited by coverage
UE distribution	Random, low density
UE speed	Up to 70 km/h
LOS/NLOS	Both
Shadow fading	Present
Channel model	COST2100
Examples	Wide area network, rural broadband access
METIS relation	TC7 “Blind spots”

Contrary to Scenarios 1–4, in this scenario UEs do not typically have high density. Hence, achieving extreme capacity by means of spatially multiplexing many users is not anymore the main driver for deployment of massive arrays at the BSs. Instead, the need is to achieve enhanced coverage and energy efficiency in non-urban areas, enabled by a relatively sparse deployment with large inter-site distances. These require massive beamforming capabilities instead of MU-MIMO, because in these situations improving coverage is more challenging than providing massive capacity. The ambition is to provide rural broadband access as a replacement to fixed wireline. Bringing effective broadband access to suburban and rural areas is one of the main objectives of 5G systems: to deliver high and sustained data rate anywhere, at any time

and with any device<sup>2</sup>. In this regard, providing good connectivity up to moderate user speeds in large areas can be efficiently addressed by massive MIMO deployments.

Examples of such scenario are wide area coverage and rural broadband access. This scenario relates to TC7 “blind spots”. The main characteristics of the scenario “wide area with mobility” are summarized in Table 1.7.

## 1.4 Baseline scenarios

### 1.4.1 Outdoor - 3GPP LTE Rel. 8

The baseline reference scenario for urban outdoor macro operation is 3GPP UMa, described in [47]. It is applicable for scenarios in urban and suburban areas outside the high rise core where the buildings are of nearly uniform height.

The mean received power in UL and DL can be expressed as:

$$RX_{PWR} = TX_{PWR} - \max(L - G_{TX} - G_{RX}, MCL)$$

where  $RX_{PWR}$  is the received signal power,  $TX_{PWR}$  is the transmitted signal power,  $L$  is the pathloss,  $G_{TX}$  is the transmitter antenna gain,  $G_{RX}$  is the receiver antenna gain and  $MCL$  is the minimum coupling loss defined by Table 1.8.

Table 1.8: Minimum coupling losses (MCL) [47].

Environment	Scenario	MCL
Macro cell Urban Area	BS - UE	70 dB
Macro cell Rural Area	BS - UE	80 dB

The pathloss  $L$  is calculated with the aid of the following expression:

$$L = 40(1 - 4 \cdot 10^{-3} Dhb) \log_{10}(R) - 18 \log_{10}(Dhb) + 21 \log_{10}(f) + 80\text{dB}$$

where  $R$  is the BS-UE separation in km,  $f$  is the carrier frequency in MHz,  $Dhb$  is the BS antenna height in m, measured from the average rooftop level.

After  $L$  is calculated, log-normally distributed large-scale fading (LogF) with standard deviation of 10 dB should be added. A shadowing correlation factor of 0.5 for the shadowing between sites and of 1 between sectors of the same site shall be used. The pathloss is given by the following formula:

$$\text{Pathloss}_{\text{macro}} = L + \text{Log}F$$

The link level performance should be analysed following the same link methodology intended for massive MIMO evaluations. Either detailed physical-layer processing or suitable abstraction models (e.g. link-to-system mechanisms) can be employed to provide fair comparison between baseline reference and massive MIMO evaluations. Applicable performance benchmarks and methodology for link-level evaluations in LTE are collected in [48]. The consortium still needs to agree on a common set of assumptions for both baseline LTE and massive MIMO evaluations so as to yield fair comparisons between both systems. To this end, only a subset of the methodology in [48] may be observed for the sake of simplicity. The outcome of such decisions will be reflected in this living document throughout the project.

<sup>2</sup>See, for example, Ericsson’s Networked Society Vision available at the following site: [http://www.ericsson.com/thinkingahead/networked\\_society](http://www.ericsson.com/thinkingahead/networked_society)

### 1.4.2 Indoor - IEEE 802.11ac

The baseline reference for indoor scenarios may be picked from [4], referring to the category of “dense networks with large numbers of stations”. Four possible indoor scenarios can be selected belonging to this category:

- Station/shopping mall
- Stadium/auditorium
- Home (dense apartments)
- Enterprise

Table in Figure 1.4 collects the five real-world scenarios considered for evaluations in IEEE High Efficiency WLAN (HEW) Study Group (SG), along with usage models.

Figure 1.5 illustrates a real-world scenario comprising several usage models. A tentative proposal of parameters from IEEE HEW SG is also provided in Table 1.6.

Scenario	Usage model	Managed?	Large no. of STAs	Large no. of APs	Outdoor
Urban outdoor	Offload to outdoor hotspots	Yes			✓
	Offload to Community Wi-Fi	Partial		✓	✓
	D2D discovery (smart cities, etc)	No	✓	✓	✓
Station / shopping mall	Offload to indoor hotspots (e.g. co-deployed with LTE picocell)	Yes		✓	
	Portal/offload to in-store AP	No		✓	
	D2D discovery (retail, etc)	No	✓	✓	
Stadium / auditorium	Portal/offload to dense hotspots	Yes	✓	✓	
	Cellular tethering	No	✓	✓	
Home (dense apartments)	Offload to home gateway, IPTV	No		✓	
	Wireless display (STB to TV, etc)	No		✓	
Enterprise	SaaS, UCC, HD video conference	Yes		✓	
	Wireless display (desktop, projector), storage and docking	No	✓	✓	
	Private APs (personal, neighbor)	No		✓	

Figure 1.4: Scenarios and usage models under consideration in IEEE HEW SG [4].

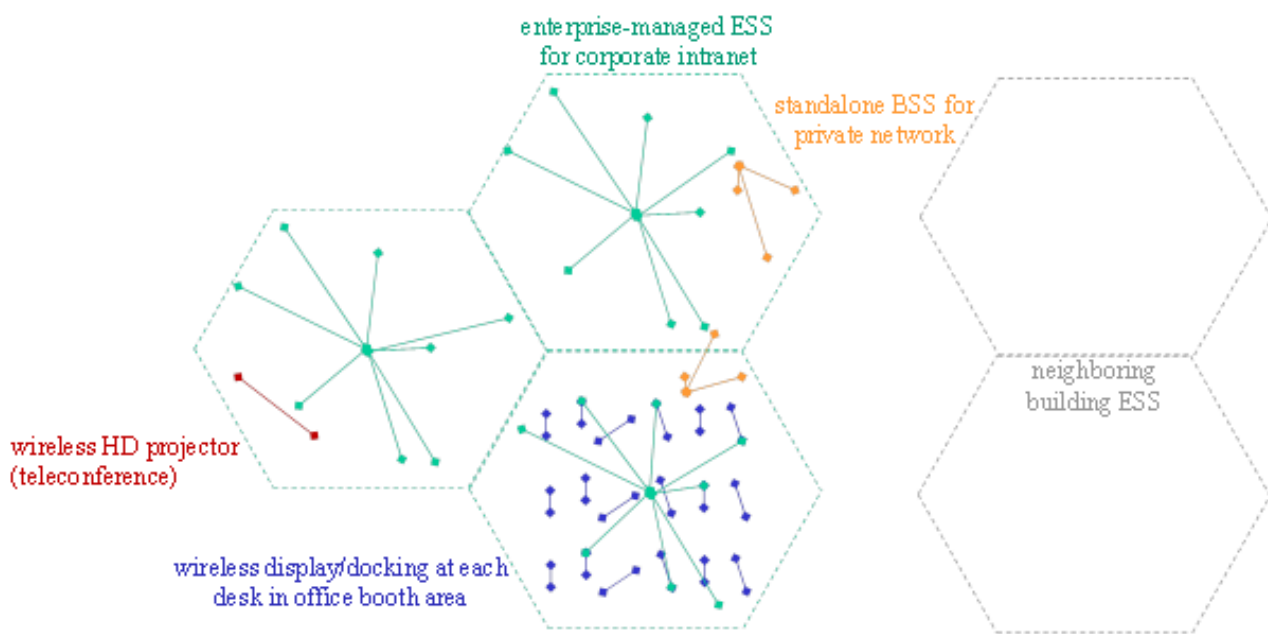


Figure 1.5: Illustration of a real-world scenario for IEEE 802.11ac evaluations [4].

Scenario	Usage model	Managed?	Topology layers
Station / shopping mall	Offload to indoor hotspots (e.g. co-deployed with LTE picocell)	Yes	1 AP/2,500m <sup>2</sup> in grid, 2-4 SPs, 50-100 STAs/AP
	Portal/offload to in-store AP	No	1 AP/625m <sup>2</sup> randomly located, 1-10 STAs/AP
	D2D discovery (retail, etc)	No	1 AP/100-1,000m <sup>2</sup> , 50-100 STAs/2,500m <sup>2</sup>
Stadium / auditorium	Portal/offload to dense hotspots	Yes	1 AP/100m <sup>2</sup> in grid, 1 SP, 50-100 STAs/AP
	Cellular tethering	No	1 AP/50m <sup>2</sup> in grid, 1-3 STAs/AP
Home (dense apartments)	VoD/IPTV and web (HGW)	No	1 AP/house randomly located, 10-50 STAs/AP
	Wireless display (e.g. STB-TV)	No	0-3 pairs/house, random AP location, STAs 2-10m from AP
Enterprise	SaaS, UCC, HD video conf.	Yes	1 AP/250m <sup>2</sup> in grid, 1 SP (+1 neighbor), 20-50 STAs/AP
	Wireless display (desktop, projector) and storage	No	0-50 pairs/250m <sup>2</sup> , STAs 0.5-3m from AP
	Private APs (personal, neighbor)	No	1-5 APs/250m <sup>2</sup> randomly located, 1-5 STAs/AP

Figure 1.6: Proposal of scenario parameters under consideration in IEEE HEW SG [4].

# Chapter 2

## Massive MIMO system outline

Cellular communication networks are continuously evolving to keep up with the rapidly increasing demand for wireless data services. Higher area throughput (in bit/s per unit area) has traditionally been achieved by a combination of three multiplicative factors [38]: more frequency spectrum (Hz), higher cell density (more cells per unit area), and higher spectral efficiency (bit/s/Hz/cell). The massive MIMO concept considered in this document was initially proposed in [35] and is envisioned to be a key technical feature of 5G systems, targeting to increase the spectral efficiency (SE) by orders of magnitude over contemporary systems [7, 17, 33]. Massive MIMO does not stand in conflict with increasing the bandwidth and the cell density, but these approaches complement one another.

The massive MIMO concept is based on equipping BSs with hundreds or thousands of antenna elements which, unlike conventional cellular technology, are operated in a phase-coherent fashion. This can provide unprecedented array gains and a spatial resolution that allows for multi-user MIMO communication to tens or hundreds of UEs per cell, while maintaining robustness to inter-user interference.

The main operation and properties of massive MIMO are described in the following sections, from a communication theoretic viewpoint. Further details on baseband processing algorithms are presented in Chapter 2 of MAMMOET deliverable D3.1 [3].

### 2.1 Basic concept and transmission protocol

Consider a cellular network with universal time and frequency reuse. Each cell is given an index in the set  $\mathcal{L}$ , where the cardinality  $|\mathcal{L}|$  is the number of cells. The BS in each cell is equipped with an array of  $M$  antennas and communicates with  $K$  single-antenna UEs in the cell. In massive MIMO topologies, the number of antennas,  $M$ , is large, but there is not exact definition.

Each UE may move around in its serving cell. The geometric position of UE  $k \in \{1, \dots, K\}$  in cell  $l \in \mathcal{L}$  is thus a random variable and denoted by  $\mathbf{z}_{lk} \in \mathbb{R}^3$ . The time-frequency resources are divided into frames consisting of  $T_c$  seconds and  $W_c$  Hz, as illustrated in Figure 2.1. This leaves room for  $S = T_c W_c$  transmission symbols per frame. We assume that the frame dimensions are such that  $T_c$  is smaller or equal to the coherence time of all UEs, while  $W_c$  is smaller or equal to the coherence bandwidth of all UEs. Hence, all the channels can be taken as static within the frame;  $\mathbf{h}_{jlk} \in \mathbb{C}^M$  denotes the channel response between UE  $k$  in cell  $l$  and BS  $j$  in a given frame.

In order to facilitate the derivation of closed-form expressions for the channel estimation error covariance and average achievable spectral efficiencies in Sections 2.4 and 2.5, respectively, we

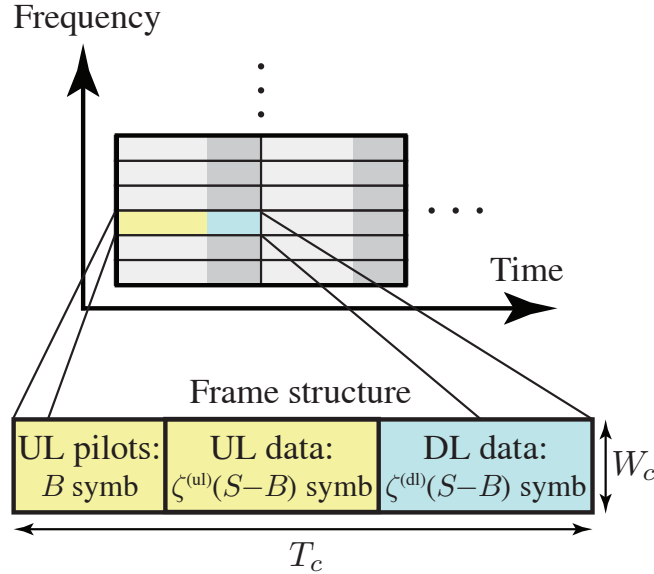


Figure 2.1: The transmission is divided into frames of  $S = T_c W_c$  symbols, whereof  $B$  symbols are dedicated to pilots. The remaining  $S - B$  symbols are used for payload data, where  $\zeta^{(ul)}$  and  $\zeta^{(dl)}$  are respectively the fractions of UL and DL transmission.

assume for the moment<sup>1</sup> that the channel responses are drawn as realizations from zero-mean circularly symmetric complex Gaussian distributions,

$$\mathbf{h}_{jlk} \sim \mathcal{CN}(\mathbf{0}, d_j(\mathbf{z}_{lk})\mathbf{I}_M), \quad (2.1)$$

where  $\mathbf{I}_M$  is the  $M \times M$  identity matrix. This is a reasonable model for non-line-of-sight propagation from arrays with both few and many antennas (see recent channel measurements reported in [27]). The deterministic function  $d_j(\mathbf{z})$  gives the mean power of the channel attenuation from BS  $j$  to any UE position  $\mathbf{z}$ . We assume that the value of  $d_j(\mathbf{z}_{lk})$  is known at BS  $j$  for all  $l$  and  $k$  (it can be measured over frequency and tracked over time), while the exact UE positions are unknown.

We consider the TDD protocol shown in Figure 2.1, where  $B \geq 1$  out of the  $S$  symbols in each frame are reserved for UL pilot signaling. There is no DL pilot signaling and no feedback of channel station information (CSI), because the system can process both UL and DL signals based on UL channel measurements due to the channel reciprocity in TDD systems. The remaining  $S - B$  symbols are thus allocated for payload data and are split between UL and DL transmission. We let  $\zeta^{(ul)}$  and  $\zeta^{(dl)}$  denote the fixed fractions allocated for UL and DL, respectively. These fractions can be selected arbitrarily, under the conditions that  $\zeta^{(ul)} + \zeta^{(dl)} = 1$  and that  $\zeta^{(ul)}(S - B)$  and  $\zeta^{(dl)}(S - B)$  are positive integers. Next, we define the system models for the uplink (UL) and downlink (DL).

## 2.2 Uplink signaling

The received UL signals  $\mathbf{y}_j \in \mathbb{C}^M$  at BS  $j$  in a frame are modeled, similar to [32, 37], as

$$\mathbf{y}_j = \sum_{l \in \mathcal{L}} \sum_{k=1}^K \sqrt{p_{lk}} \mathbf{h}_{jlk} x_{lk} + \mathbf{n}_j \quad (2.2)$$

<sup>1</sup>Channel measurements are currently ongoing in MAMMOET, aiming to yield in mid 2015 an accurate massive MIMO channel model.

where  $x_{lk} \in \mathbb{C}$  is the symbol transmitted by UE  $k$  in cell  $l$ . This signal is normalized as  $\mathbb{E}\{|x_{lk}|^2\} = 1$ , while the corresponding UL transmit power is defined by  $p_{lk} \geq 0$ . The additive noise  $\mathbf{n}_j \in \mathbb{C}^M$  is modeled as  $\mathbf{n}_j \sim \mathcal{CN}(\mathbf{0}, \sigma^2 \mathbf{I}_M)$ , where  $\sigma^2$  is the noise variance.

Contrary to most previous works on massive MIMO, which assume fixed UL power, we consider statistics-aware power control<sup>2</sup>; the symbols from UE  $k$  in cell  $l$  have the transmit power  $p_{lk} = \frac{\rho}{d_l(\mathbf{z}_{lk})}$ , where  $\rho > 0$  is a design parameter. This power-control policy inverts the average channel attenuation  $d_l(\mathbf{z}_{lk})$  and has the merit of making the average effective channel gain the same for all UEs:  $\mathbb{E}\{p_{lk} \|\mathbf{h}_{lk}\|^2\} = M\rho$ . Hence, this policy guarantees a uniform user experience, saves valuable energy at UEs, and avoids near-far blockage where weak signals drown in stronger signals due to the finite dynamic range of analog-to-digital converters (ADCs) of the BS.

## 2.3 Downlink signaling

Building on the uplink-downlink channel reciprocity in calibrated TDD systems, see [49], the received DL signal  $z_{jk} \in \mathbb{C}$  at UE  $k$  in cell  $j$  in a frame is modeled as

$$z_{jk} = \sum_{l \in \mathcal{L}} \sum_{m=1}^K \mathbf{h}_{ljk}^T \mathbf{w}_{lm} s_{lm} + \eta_{jk} \quad (2.3)$$

where  $s_{lm}$  is the symbol intended for UE  $m$  in cell  $l$  and  $\mathbf{w}_{lm} \in \mathbb{C}^M$  is the corresponding linear precoding vector. The corresponding DL transmit power is given by  $\|\mathbf{w}_{lm}\|^2$ . Any power control can be considered in the DL since it has access to the CSI acquired on the UL, but we will show later how to select the transmit power to achieve the same SEs in the DL as in the UL. The additive noise at UE  $k$  in cell  $j$  is modeled as  $\eta_{jk} \sim \mathcal{CN}(\mathbf{0}, \sigma^2)$ , where the variance is the same as in the UL.

## 2.4 Pilot-based channel estimation

BS  $j$  can use its multitude of antennas for phase-coherent receive combining in the UL and transmit precoding in the DL, which can adaptively amplify desired signals and can suppress interfering signals. This requires, however, some knowledge of the UEs' channels; for example,  $\sqrt{p_{lk}} \mathbf{h}_{ljk}$  in the UL, for all  $l$  and  $k$ . Such CSI is typically acquired by pilot signaling, where the UEs send known signals. Accurate CSI acquisition is a challenging task in networks where the transmission resources are reused across cells, because the pilot signals are inevitably affected by inter-cell interference. This so-called *pilot contamination* limits the quality of the acquired CSI and the ability to reject inter-cell interference (unless intricate subspace methods can be used for decontamination, as suggested in [36]).

The impact of pilot contamination is usually studied under the assumption that exactly the same pilot signals are used in all cells, but from a performance optimization perspective it might be better that each cell only uses a subset of the pilots. Hence, we consider a general pilot allocation, where the pilot signals are assumed to span  $B$  symbols of the frame, for  $1 \leq B \leq S$ , and each cell uses  $K$  of these pilot signals. Each pilot signal can be represented

<sup>2</sup>Channel-aware (a.k.a. closed-loop) power control was considered in [15, 30], but it requires a rapid feedback mechanism where UEs are provided with instantaneous CSI. Since the small-scale fading averages out in massive MIMO systems, we expect statistical power control policies to be almost equal to channel-aware policies, but considerably easier to implement.

by a deterministic vector  $\mathbf{v} \in \mathbb{C}^B$  and the fixed per-symbol power implies that all entries have unit magnitude:  $|\mathbf{v}_s| = 1$ , where  $[\cdot]_s$  denotes the  $s$ th element for  $s \in \{1, \dots, B\}$ . We assume that all pilot signals originate from a fixed *pilot book*  $\mathcal{V}$ , defined as

$$\mathcal{V} = \{\mathbf{v}_1, \dots, \mathbf{v}_B\} \quad \text{where} \quad \mathbf{v}_{b_1}^H \mathbf{v}_{b_2} = \begin{cases} B, & b_1 = b_2, \\ 0, & b_1 \neq b_2. \end{cases} \quad (2.4)$$

Hence, the  $B$  pilot signals form an orthogonal basis and can, for example, be taken as the columns of a discrete Fourier transform (DFT) matrix [8]. The pilot signal transmitted by UE  $k$  in cell  $l$  is denoted as  $\mathbf{v}_{i_{lk}}$ , where  $i_{lk} \in \{1, \dots, B\}$  is the index in the pilot book.

By transmitting these pilot signals over  $B$  symbols in the UL system model of (2.5), the collective received UL signal at BS  $j$  is denoted as  $\mathbf{Y}_j \in \mathbb{C}^{M \times B}$  and given by

$$\mathbf{Y}_j = \sum_{l \in \mathcal{L}} \sum_{k=1}^K \sqrt{p_{lk}} \mathbf{v}_{i_{lk}}^T + \mathbf{N}_j, \quad (2.5)$$

where  $\mathbf{N}_j \in \mathbb{C}^{M \times B}$  contains the additive noise at the receiver during the pilot signaling.

The following lemma from [13] derives the minimum mean-squared error (MMSE) estimator of the effective power-controlled UL channels, which are defined as  $\mathbf{h}_{jlk}^{\text{eff}} = \sqrt{p_{lk}} \mathbf{h}_{jlk}$ .

**Lemma 1.** *The MMSE estimate at BS  $j$  of the effective power-controlled UL channel  $\mathbf{h}_{jlk}^{\text{eff}}$ , for any UE  $k \in \{1, \dots, K\}$  in any cell  $l \in \mathcal{L}$ , is*

$$\hat{\mathbf{h}}_{jlk}^{\text{eff}} = \frac{d_j(\mathbf{z}_{lk})}{d_l(\mathbf{z}_{lk})} \mathbf{Y}_j \boldsymbol{\Psi}_j^{-1} \mathbf{v}_{i_{lk}}^* \quad (2.6)$$

where  $(\cdot)^*$  denotes the complex conjugate and the normalized covariance matrix  $\boldsymbol{\Psi}_j \in \mathbb{C}^{B \times B}$  of the received signal is

$$\boldsymbol{\Psi}_j = \sum_{\ell \in \mathcal{L}} \sum_{m=1}^K \frac{d_j(\mathbf{z}_{\ell m})}{d_\ell(\mathbf{z}_{\ell m})} \mathbf{v}_{i_{\ell m}} \mathbf{v}_{i_{\ell m}}^H + \frac{\sigma^2}{\rho} \mathbf{I}_B. \quad (2.7)$$

The estimation error covariance matrix  $\mathbf{C}_{jlk} \in \mathbb{C}^{M \times M}$  is given by

$$\begin{aligned} \mathbf{C}_{jlk} &= \mathbb{E} \left\{ (\mathbf{h}_{jlk}^{\text{eff}} - \hat{\mathbf{h}}_{jlk}^{\text{eff}}) (\mathbf{h}_{jlk}^{\text{eff}} - \hat{\mathbf{h}}_{jlk}^{\text{eff}})^H \right\} \\ &= \rho \frac{d_j(\mathbf{z}_{lk})}{d_l(\mathbf{z}_{lk})} \left( 1 - \frac{\frac{d_j(\mathbf{z}_{lk})}{d_l(\mathbf{z}_{lk})} B}{\sum_{\ell \in \mathcal{L}} \sum_{m=1}^K \frac{d_j(\mathbf{z}_{\ell m})}{d_\ell(\mathbf{z}_{\ell m})} \mathbf{v}_{i_{\ell m}}^H \mathbf{v}_{i_{\ell m}} + \frac{\sigma^2}{\rho}} \right) \mathbf{I}_M \end{aligned} \quad (2.8)$$

and the mean-squared error (MSE) is  $\text{MSE}_{jlk} = \text{tr}(\mathbf{C}_{jlk})$ .

Looking at the estimation error covariance matrix  $\mathbf{C}_{jlk}$  in (2.8), we see that the error depends only on the inverse signal-to-noise ratio (SNR),  $\sigma^2/\rho$ , and on which UEs that have been allocated the same pilot signal (i.e., which of the products  $\mathbf{v}_{i_{lk}}^H \mathbf{v}_{i_{\ell m}}$  that are non-zero). The ratio  $d_j(\mathbf{z}_{\ell m})/d_\ell(\mathbf{z}_{\ell m})$  determines the relative strength of the interference received at BS  $j$  from UE  $m$  in cell  $\ell$ ; it is almost one for cell-edge UEs of neighboring cells, while it is almost zero when cell  $\ell$  is very distant from BS  $j$ .

Although Lemma 1 allows for estimation of all channel vectors in the whole cellular network, each BS can only resolve  $B$  different spatial dimensions since there are only  $B$  orthogonal pilot signals. To show this explicitly, we define the  $M \times B$  matrix

$$\hat{\mathbf{H}}_{\mathcal{V},j} = \mathbf{Y}_j \boldsymbol{\Psi}_j^{-1} [\mathbf{v}_1^* \dots, \mathbf{v}_B^*] \quad (2.9)$$

using each of the  $B$  pilot signals from  $\mathcal{V}$ . The channel estimate in (2.6) for UE  $k$  in cell  $l$  is parallel to the  $i_{lk}$ th column of  $\widehat{\mathbf{H}}_{\mathcal{V},j}$ ; more precisely, we have

$$\hat{\mathbf{h}}_{jlk}^{\text{eff}} = \frac{d_j(\mathbf{z}_{lk})}{d_l(\mathbf{z}_{lk})} \widehat{\mathbf{H}}_{\mathcal{V},j} \mathbf{e}_{i_{lk}} \quad (2.10)$$

where  $\mathbf{e}_i$  denotes the  $i$ th column of the  $B \times B$  identity matrix  $\mathbf{I}_B$ . This is the essence of pilot contamination; BSs cannot tell apart UEs that use the same pilot signal and thus cannot reject the corresponding interference. In some cases (e.g., for slow changes in the user scheduling and high spatial channel correlation), user-specific statistical prior knowledge can be utilized to partially separate the UEs [53], but this will not be considered herein since we aim at establishing fundamental system properties that can be exploited in any propagation environment.

## 2.5 Average achievable spectral efficiencies

The channel estimates in Lemma 1 enable each BS to (semi-)coherently detect the data signals from its UEs. In particular, we assume that BS  $j$  applies a linear receive combining vector  $\mathbf{g}_{jk} \in \mathbb{C}^M$  to the received signal, as  $\mathbf{g}_{jk}^H \mathbf{y}_j$ , to amplify the signal from its  $k$ th UE and reject interference from other UEs in the spatial domain.

The combining schemes for massive MIMO can have either *passive* or *active* interference rejection. The canonical example of passive rejection is maximum ratio (MR) combining, defined as

$$\mathbf{g}_{jk}^{\text{MR}} = \widehat{\mathbf{H}}_{\mathcal{V},j} \mathbf{e}_{i_{jk}} = \hat{\mathbf{h}}_{jjk}^{\text{eff}}, \quad (2.11)$$

which maximizes the gain of the desired signal and relies on that interfering signals are rejected automatically since the co-user channels are quasi-orthogonal to  $\hat{\mathbf{h}}_{jjk}^{\text{eff}}$  when  $M$  is large.<sup>3</sup>

In contrast, active rejection is achieved by making the receive combining as orthogonal to the interfering channels as possible. This is conventionally achieved by zero-forcing (ZF) combining, where the combining is selected to orthogonalize the  $K$  intra-cell channels:

$$\mathbf{g}_{jk}^{\text{ZF}} = \widehat{\mathbf{H}}_{\mathcal{V},j} \mathbf{E}_j (\mathbf{E}_j^H \widehat{\mathbf{H}}_{\mathcal{V},j}^H \widehat{\mathbf{H}}_{\mathcal{V},j} \mathbf{E}_j)^{-1} \mathbf{e}_{i_{jk}}, \quad (2.12)$$

where  $\mathbf{E}_j = [\mathbf{e}_{i_{j1}} \dots \mathbf{e}_{i_{jK}}] \in \mathbb{C}^{B \times K}$  and all the UEs in cell  $j$  are required to use different pilots.

ZF combining only actively suppresses intra-cell interference, while the inter-cell interference is passively suppressed as in MR combining. Further interference rejection can be achieved by coordinating the combining across cells, such that both intra-cell and inter-cell interference are actively suppressed by the receive combining. We propose a new *full pilot-based zero-forcing (P-ZF) combining*, defined as

$$\mathbf{g}_{jk}^{\text{P-ZF}} = \widehat{\mathbf{H}}_{\mathcal{V},j} (\widehat{\mathbf{H}}_{\mathcal{V},j}^H \widehat{\mathbf{H}}_{\mathcal{V},j})^{-1} \mathbf{e}_{i_{jk}}. \quad (2.13)$$

In contrast to the conventional ZF in (2.12), which only orthogonalizes the  $K$  intra-cell channels in  $\widehat{\mathbf{H}}_{\mathcal{V},j} \mathbf{E}_j$ , P-ZF exploits that all the  $B$  estimated channel directions in  $\widehat{\mathbf{H}}_{\mathcal{V},j}$  are known at BS  $j$  and orthogonalizes all of them to also mitigate parts of the inter-cell interference. The cost is a loss in array gain of  $B$ , instead of  $K$  as in ZF. Note that there is no signaling between BS in this coordinated multipoint (CoMP) scheme—BS  $j$  estimates  $\widehat{\mathbf{H}}_{\mathcal{V},j}$  from the UL pilot signaling—and thus the P-ZF scheme is fully scalable.

<sup>3</sup>With *quasi-orthogonality* we mean that two vectors  $\mathbf{a}, \mathbf{b} \in \mathbb{C}^M$  satisfy  $\frac{\mathbf{a}^H \mathbf{b}}{M} \rightarrow 0$  as  $M \rightarrow \infty$ , although  $\mathbf{a}^H \mathbf{b}$  will not converge to zero and might even go to infinity, e.g., proportionally to  $\sqrt{M}$  as with Rayleigh fading channel vectors.

In the DL, the channel estimates are used for linear precoding in the DL, where the  $M$  channel inputs are utilized to make each data signal add up (semi-)coherently at its desired UE and to suppress inter-user interference at other UEs. Recall from (2.3) that  $\mathbf{w}_{jk} \in \mathbb{C}^M$  is the precoding vector allocated for UE  $k$  in cell  $j$ . In this document, we define the precoding vectors as

$$\mathbf{w}_{jk} = \sqrt{\frac{q_{jk}}{\mathbb{E}_{\{\mathbf{h}\}}\{\|\check{\mathbf{g}}_{jk}\|^2\}}} \check{\mathbf{g}}_{jk}^* \quad (2.14)$$

where the average transmit power  $q_{jk} \geq 0$  is a function of the UE positions, but not the instantaneous channel realizations. The vector  $\check{\mathbf{g}}_{jk} \in \mathbb{C}^M$  defines the spatial directivity of the transmission and is based on the acquired CSI. This vector is usually selected in the same way as the receive combining; more precisely, MR precoding which amplifies the desired is obtained by setting  $\check{\mathbf{g}}_{jk} = \mathbf{g}_{jk}^{\text{MR}}$ ; ZF precoding that actively rejects intra-cell interference is achieved by setting  $\check{\mathbf{g}}_{jk} = \mathbf{g}_{jk}^{\text{ZF}}$ ; and P-ZF precoding that actively rejects both intra- and inter-cell interference is achieved by setting  $\check{\mathbf{g}}_{jk} = \mathbf{g}_{jk}^{\text{P-ZF}}$ . The reason for this is the uplink-downlink duality [18], which says that the same performance can be achieved in the UL and DL by using the same processing vectors,  $\check{\mathbf{g}}_{jk} = \mathbf{g}_{jk}$ , and only modifying the power allocation.

Having defined the linear processing in the UL and DL, we have the following result from [12].

**Theorem 1.** *Looking jointly at the UL and DL, an achievable SE for UE  $k$  in cell  $j$  is*

$$\text{SE}_{jk} = \left(1 - \frac{B}{S}\right) \log_2 \left(1 + \frac{B}{I_{jk}^{\text{scheme}}}\right) \quad [\text{bit/s/Hz/user}]. \quad (2.15)$$

where the interference term  $I_{jk}^{\text{scheme}}$  depends on the linear processing scheme.

MR processing gives

$$\begin{aligned} I_{jk}^{\text{MR}} = & \sum_{l \in \mathcal{L}} \sum_{\substack{m=1 \\ (l,m) \neq (j,k)}}^K \left( \mu_{jl}^{(2)} + \frac{\mu_{jl}^{(2)} - (\mu_{jl}^{(1)})^2}{M} \right) \mathbf{v}_{i_{jk}}^H \mathbf{v}_{i_{lm}} \\ & + \left( \sum_{l \in \mathcal{L}} \mu_{jl}^{(1)} \frac{K}{M} + \frac{\sigma^2}{M\rho} \right) \left( \sum_{\ell \in \mathcal{L}} \sum_{m=1}^K \mu_{j\ell}^{(1)} \mathbf{v}_{i_{jk}}^H \mathbf{v}_{i_{\ell m}} + \frac{\sigma^2}{\rho} \right) \end{aligned} \quad (2.16)$$

ZF processing gives

$$\begin{aligned} I_{jk}^{\text{ZF}} = & \sum_{l \in \mathcal{L}} \sum_{\substack{m=1 \\ (l,m) \neq (j,k)}}^K \left( \mu_{jl}^{(2)} + \frac{\mu_{jl}^{(2)} - (\mu_{jl}^{(1)})^2}{M - K} \right) \mathbf{v}_{i_{jk}}^H \mathbf{v}_{i_{lm}} \\ & + \left( \sum_{l \in \mathcal{L}} \sum_{m=1}^K \mu_{jl}^{(1)} \left( 1 - \frac{\mu_{jl}^{(1)} \sum_{\tilde{k}=1}^K \mathbf{v}_{i_{j\tilde{k}}}^H \mathbf{v}_{i_{lm}}}{\sum_{\ell \in \mathcal{L}} \sum_{\tilde{m}=1}^K \mu_{j\ell}^{(1)} \mathbf{v}_{i_{lm}}^H \mathbf{v}_{i_{\ell\tilde{m}}} + \frac{\sigma^2}{\rho}} \right) + \frac{\sigma^2}{\rho} \right) \left( \frac{\sum_{\ell \in \mathcal{L}} \sum_{m=1}^K \mu_{j\ell}^{(1)} \mathbf{v}_{i_{jk}}^H \mathbf{v}_{i_{\ell m}} + \frac{\sigma^2}{\rho}}{M - K} \right), \end{aligned} \quad (2.17)$$

and P-ZF processing gives

$$\begin{aligned}
I_{jk}^{\text{P-ZF}} = & \sum_{l \in \mathcal{L}} \sum_{\substack{m=1 \\ (l,m) \neq (j,k)}}^K \left( \mu_{jl}^{(2)} + \frac{\mu_{jl}^{(2)} - (\mu_{jl}^{(1)})^2}{M - B} \right) \mathbf{v}_{i_{jk}}^H \mathbf{v}_{i_{lm}} \\
& + \left( \sum_{l \in \mathcal{L}} \sum_{m=1}^K \mu_{jl}^{(1)} \left( 1 - \frac{B \mu_{jl}^{(1)}}{\sum_{\ell \in \mathcal{L}} \sum_{\tilde{m}=1}^K \mu_{j\ell}^{(1)} \mathbf{v}_{i_{lm}}^H \mathbf{v}_{i_{\ell\tilde{m}}} + \frac{\sigma^2}{\rho}} \right) + \frac{\sigma^2}{\rho} \right) \left( \frac{\sum_{\ell \in \mathcal{L}} \sum_{m=1}^K \mu_{j\ell}^{(1)} \mathbf{v}_{i_{jk}}^H \mathbf{v}_{i_{\ell m}} + \frac{\sigma^2}{\rho}}{M - B} \right). \tag{2.18}
\end{aligned}$$

The following notation was used:

$$\mu_{jl}^{(\gamma)} = \mathbb{E}_{\mathbf{z}_{lm}} \left\{ \left( \frac{d_j(\mathbf{z}_{lm})}{d_l(\mathbf{z}_{lm})} \right)^\gamma \right\} \quad \text{for } \gamma = 1, 2. \tag{2.19}$$

The first term in each of (2.16)–(2.18) describes the pilot contamination, while the second term is the inter-user interference. The SE in (1) can be divided between the UL and DL arbitrarily using the fractions  $\zeta^{(\text{ul})}$  and  $\zeta^{(\text{dl})}$ ; more precisely,  $\zeta^{(\text{ul})}\text{SE}_{jk}$  is the SE in the UL and  $\zeta^{(\text{dl})}\text{SE}_{jk}$  is the SE in the DL. The fact that the SE expression is essentially the same for the UL and DL is very convenient, since it allows us to analyze and optimize the performance of the network as a whole.

The closed-form SE expressions in Theorem 1 are only functions of the pilot allocation and the propagation parameters  $\mu_{jl}^{(1)}$  and  $\mu_{jl}^{(2)}$ . The latter two are the average ratio between the channel variance to BS  $j$  and the channel variance to BS  $l$ , for an arbitrary UE in cell  $l$ , and the second-order moment of this ratio, respectively. The SE expressions manifest the importance of pilot allocation, since all the interference terms in (2.16) and (2.17) contain inner products of pilot signals that are either equal to zero or  $B$ .

# Chapter 3

## Performance metrics

In order to properly evaluate massive MIMO solutions, it is important to model the achievable throughput at different system levels (per user, cell, and area) as well as the corresponding power consumption. There is thus a variety of different performance metrics and aspects that can be considered in the design of future networks [11]. The main metrics considered in this document are:

- Spectral efficiency per cell [bit/s/Hz/cell];
- Fairness among UEs;
- Total energy efficiency [bit/Joule].

Further performance metrics could be the bit error rate, outage probability, total power consumption, etc.

A key property of massive MIMO is that a high degree of fairness can be ensured by computationally efficient and robust power allocation schemes, which only depend on the channel statistics and not on the instantaneous channel realizations in each frame. In fact, the per-user SE expression in Theorem 1 in Section 2.5 is independent of the UE locations and only depend on how the  $B$  pilots are allocated across cells. If the pilot allocation is symmetric and fair, then all UEs in every cell will achieve the same SEs.

For this reason, we consider the fairness problem as relatively easier to be solved by the massive MIMO architecture and concentrate on the SE per cell and on the total energy efficiency. Expressions for the SEs were developed in Theorem 1 in Section 2.5, but the power consumption remains to modeled.

### 3.1 Modeling of total power in massive MIMO systems

Given the fundamental differences between massive MIMO BSs and traditional (macro) BSs, estimating their power consumption requires a significant modeling effort, taking into account all the different components in order to assess the total system power consumption. Power modeling for massive MIMO has been considered in [15, 25, 52]. In this section, we summarize the way to evaluate the power consumption proposed in [25]. This model also builds on prior power modeling effort in [23, 24] for different types of cellular BSs.

One main assumption is made in order to guide the power modeling: given the large number of transmit antennas in massive MIMO systems, every single antenna chain does not require to generate very accurate signals, thanks to an averaging effect of the non-idealities achieved

by precoding/combining all the antennas. Two principles support this assumption. Firstly, while useful signals are added in phase thanks to the coherent linear processing, uncorrelated impairments are added incoherently, giving an improvement of the signal-to-impairment ratio proportional to the number of antennas  $M$  [9, 14]. Secondly, the absolute power level of the BS is reduced [15], which means that an absolute constraint on out-of-band leakage will appear less severe in relative terms with respect to the in-band signal, and additionally also benefit from the non-coherent addition of terms coming from the different antennas. The consequence of this assumption is that, despite the objective for massive MIMO to provide a coverage comparable to macro BSs, the requirements and power levels of most hardware components will be closer to those observed in smaller (pico or femto) BSs, with simpler architectures and dedicated lower-power components.

In order to model the total power consumption, the different components are modeled separately, each of them getting a specific model described in this section.

### 3.1.1 Power amplifier

The target in [25] is for massive MIMO to keep the coverage of a traditional macro BS. By reasoning on the scaling of the link budget, a coverage equivalent to a macro BS using  $4 \times 4$  MIMO and 49 dBm total output power would be achieved in a massive MIMO system with  $K = 30$  UEs,  $M = 200$  antennas at the BS and 18 dBm per antenna. Moreover, massive MIMO systems are expected to operate at a somewhat reduced spectral efficiency (per data stream). Note that the spatial multiplexing will still offer high average rates/user, improving the total throughput thanks to the large number scheduled UEs and not by using high-order constellations; see Section 4.2.2. Hence, the actual required output power level per antenna should be smaller than 18 dBm and most likely close to some 10 dBm/antenna; particularly for MR precoding as shown in [15].

Thanks to this low per-antenna output power level, massive MIMO systems do not require external power amplifiers (PAs) at the BSs. Instead, the last buffer stage of the analog front-end, the predriver, is sufficient to generate the required output power. Hence, no PA power consumption is accounted for in the model, but only the predriver power consumption. The power consumption is thus modeled in the same way as for the predriver of a small conventional base (see Section 3.1.2). The only difference is that the model makes sure that the predriver is at least able to deliver the required power level with an efficiency,  $\nu$ , set to a maximum of 50%. Hence, if the required per-antenna output power is larger than half of the predriver power consumption, its power consumption is increased to twice the antenna output power.

Obtaining a  $\nu = 0.5$  power efficiency is hardly possible while preserving a decent linearity or back-off. However, considering first the steadily improving efficiencies of amplifier architectures, not only at saturation but also at reduced output power, and secondly because we expect massive MIMO systems to tolerate a larger amount of non-linear distortion than traditional systems, this efficiency level seems achievable for future massive MIMO BSs. The innovative transmitter work in MAMMOET WP2 (see Section 3.1.6) points to this direction.

### 3.1.2 Analog front-end

The analog front-end of a massive MIMO BS contains a number of relevant sub-components. The frequency synthesizer and clock generation are active in both UL and DL. Predrivers, modulators, and digital-to-analog converters (DACs) are only used in the DL, while low-noise amplifiers (LNAs), mixers, variable-gain amplifiers (VGAs), and analog-to-digital converters

Table 3.1: Reference power consumption of analog sub-components (2012).

Subcomponent	Downlink [mW]	Uplink [mW]
Predriver	115	0
Modulator	200	0
Frequency synthesis	125	125
Clock generation	75	75
DAC	225	0
LNA	0	125
Mixer	0	200
VGA	0	63
ADC	0	175

(ADCs) are only used in the UL. Table 3.1 provides examples of the power consumption of these analog sub-components, for a reference scenario which assumes 20 MHz, a single antenna, and 24 bit quantization.

The power consumption of the analog front-end scales with three design parameters: bandwidth  $W$ , number of antennas  $M$ , and digital quantization resolution  $Q$ . Most of the power consumption values scale linearly with the bandwidth as well as with the number of antennas. Exceptions are the frequency synthesis, only scaling with antennas but not with the bandwidth, and the clock generation, also not scaling with the bandwidth and only with the square root of the number of antennas:  $\sqrt{M}$ .<sup>1</sup> Finally, DAC and ADC components additionally scale linearly with the digital quantization resolution.

Those scaling rules are implemented by the following equation, denoting  $\mathcal{I}_{\text{Analog}}$  the set of sub-components  $i$  (predriver, modulator, ...),  $\mathcal{X}_{\text{Analog}} = \{W, M, Q\}$  the set of scenario parameters  $x$  (bandwidth, antennas, and quantization resolution) having each a reference value  $x_{\text{ref}}$  and an actual value  $x_{\text{act}}$ ,  $s_{i,x}$  the scaling exponent for sub-component  $i$  with respect to parameter  $x$ ,  $P_{i,\text{ref}}$  the reference power of sub-component  $i$  and  $P_{\text{Analog}}$  the computed total power for the analog front-end:

$$P_{\text{Analog}} = \sum_{i \in \mathcal{I}_{\text{Analog}}} P_{i,\text{ref}} \prod_{x \in \mathcal{X}_{\text{Analog}}} \left( \frac{x_{\text{act}}}{x_{\text{ref}}} \right)^{s_{i,x}} \quad (3.1)$$

The reference power  $P_{i,\text{ref}}$  weighs the UL and DL power, using the corresponding fractions  $\zeta^{(\text{ul})}$  and  $\zeta^{(\text{dl})}$ . The scaling exponents  $s_{i,x}$  have value 1 for linear scaling, 0 for no scaling (fixed power with respect to the selected parameter), 0.5 for scaling with the square root of the corresponding parameter, and so on.

The power consumption also decreases over the years thanks to the evolution of silicon technology as well as architectural improvements. Although this effect differs from component to component, an average power reduction factor of  $\sqrt{2}$  was selected for analog components per new technology generation, which is currently every 2 years. This is in principle true for all systems; not massive MIMO specific.

### 3.1.3 Digital baseband

A large number of signal processing operations takes place in the digital baseband; for example, filtering, sampling, OFDM modulation/demodulation, channel coding, precoding/combining,

<sup>1</sup>The clock generation itself does not need to scale but some additional amplification is required in order to distribute the clock signal to the different antennas.

etc. The power consumption of these sub-components is modeled in a way similar to the analog sub-components, but depends on a number of additional scenario parameters. The digital power consumption is modeled through the digital complexity in terms of Giga-operations per second (GOPS); complexity values are then translated into power consumption values as function of the intrinsic efficiency of the hardware, measured in GOPS/W.

The digital sub-components are affected by some additional parameters which do not impact analog sub-components. More precisely, the power consumption scales with respect to the system load  $\Upsilon$  (in the frequency-domain), number of UEs  $K$ , and the spectral efficiency  $SE_u$  that is assigned to each UE. This leads to the following total power model for the digital baseband:

$$P_{\text{Baseband}} = \sum_{i \in \mathcal{I}_{\text{Baseband}}} P_{i,\text{ref}} \prod_{x \in \mathcal{X}_{\text{Baseband}}} \left( \frac{x_{\text{act}}}{x_{\text{ref}}} \right)^{s_{i,x}} \quad (3.2)$$

where  $\mathcal{I}_{\text{Baseband}}$  is the set of digital sub-components and  $\mathcal{X}_{\text{Baseband}} = \{W, SE_u, M, \Upsilon, K, Q\}$  is the set of scenario parameters that effect the baseband power consumption. For sub-component  $i \in \mathcal{I}_{\text{Baseband}}$ ,  $x_{\text{ref}}$  is a reference value and  $x_{\text{act}}$  is the actual value with respect to parameter  $x \in \mathcal{X}_{\text{Baseband}}$ , while  $s_{i,x}$  the corresponding scaling exponent. Further details on this power model are provided in the MAMMOET deliverable D3.1 [3]. The reference power  $P_{i,\text{ref}}$  weighs the UL and DL power, using the corresponding fractions  $\zeta^{(\text{ul})}$  and  $\zeta^{(\text{dl})}$ .

Generally speaking, the digital scaling shows more diversity over the different sub-components than the analog scaling, since  $\mathcal{X}_{\text{Baseband}}$  contains more scenario parameters than  $\mathcal{X}_{\text{Analog}}$ . Notice that the choice of precoding/combining scheme only impacts the digital baseband processing.

The technology scaling has more impact on the digital power consumption than on the analog power consumption. It is modeled by an average factor 2 of improvement in power consumption every new generation.

Next to physical-layer digital signal processing, some digital operations are also required for control of the system as well as for some higher-layer (network) processing. Those can be modeled together with the digital baseband part in (3.2).

### 3.1.4 Power system

Power system components (i.e., AC/DC and DC/DC converters) also need to be taken into account in the power model. These can typically be modeled as having 8% losses each; that is, 92% of their power consumption gets transferred to the other components in the system.

### 3.1.5 Current estimates and further developments

By considering the scenarios and modeling approach in [25], the power consumption of a  $200 \times 30$  massive MIMO BS has been extrapolated to an average of 44 W in 2020. The DL consumption of 54 W is dominated by the PA (pre-driver) (25 W) and the analog front-end (18 W). In UL the average power consumption of 34 W is dominated by the analog front-end (27 W). The digital power consumption is very limited (2 to 3 W), especially thanks to the deep technology scaling up to 2020 but also based on the selected low-complexity approach using MR precoding/combining and low quantization resolution. Power systems supporting the BS consume around 7 W.

In order to refine the accuracy of the power model described above, and hence the conclusions derived from it on the energy efficiency of massive MIMO systems, a number of elements influencing the power consumption need further attention:

1. The assumption taken on using low-cost, low-accuracy antenna chains must be further quantified; that is, how far can one reduce the specifications while still meeting the performance expectations and is the averaging of the distortions from various impairments effectively enabling to keep the desired performance despite the lower accuracy. On-going work and initial results in MAMMOET WP3 are promising.
2. The digital power consumption should be revisited and tailored to the algorithmic choices of each particular implementation; for example, the choice of precoding, hardware technology, and platform type selection.
3. The scaling of the output power with respect to the number of antennas should be validated for different relevant propagation scenarios and coverage areas.

In addition, MAMMOET WP2 develops innovative transmitter architectures that can be integrated into the model. The key features of this model are described in the next section.

### 3.1.6 Alternative transmitter architecture

The focus of MAMMOET WP2 is to provide a feasibility study of new RF transmitters that might be particularly suited for massive MIMO systems. The major requirement on the transmitters is to significantly reduce the hardware complexity and power consumption and to also increase the integration capabilities. Compared to conventional solutions based on dedicated DACs and analog IQ mixers, as shown in Figure 3.1, the new transmitter concept should also provide higher flexibility, re-configurability, and the possibility to drive efficient switched-mode RF PAs (e.g., of Class E).

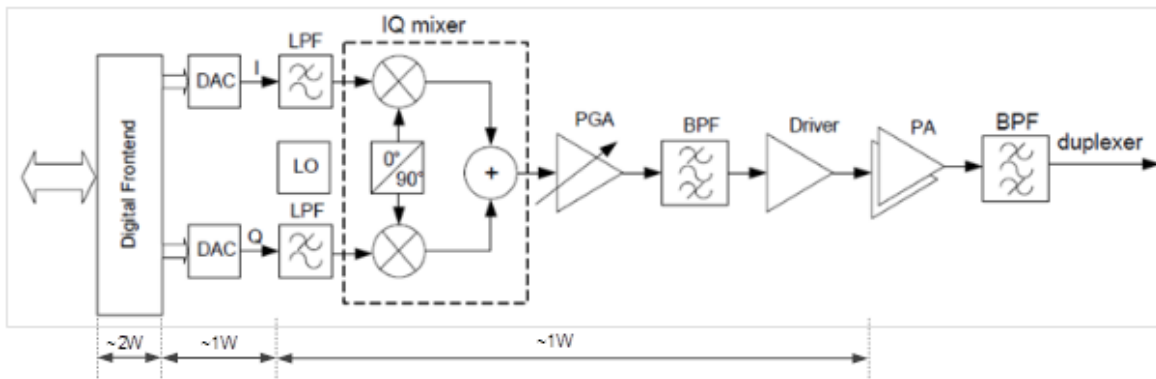


Figure 3.1: “Conventional” transmitter (with DFE+DAC+mixer+LO+PGA+Driver+SAWs).

In the innovative transmitter architecture, shown in Figure 3.2, no dedicated DACs and mixers are needed to generate the required RF driving signals for the PA. The baseband IQ signal from the digital front-end with non-constant envelope will be encoded in different purely phase-modulated signals which can easily be combined to radio-frequency pulse-width modulation (RF-PWM) signals. If conventional RF PAs are considered, band-pass filtering of the RF-PWM signals is required before the PA. In case of switched-mode PAs, the generated signals can be used directly which reduces the required RF components further. An estimate of the power consumption for the conventional solution and the new digital transmitter is provided in Table 3.2.

The key features of the new transmitter architecture are:

- simple re-configurability to adjust to different signal bandwidths and carrier frequencies;

- ability to operate with switched-mode PAs;
- lower power consumption;
- higher integration capabilities;
- inherent precoding capabilities.

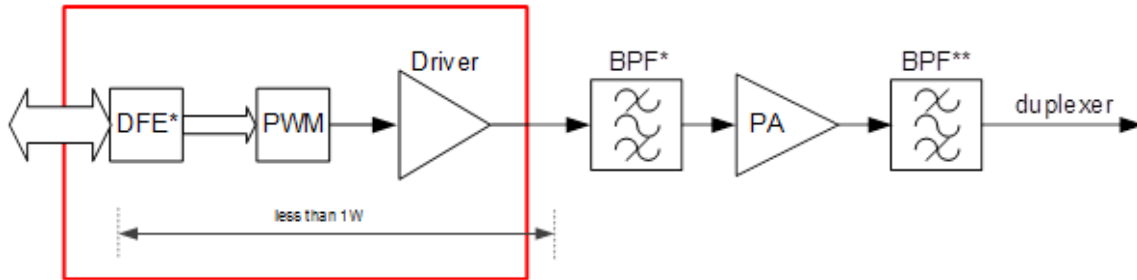


Figure 3.2: Digital RF modulator on a chip.

Table 3.2: Power consumption: conventional and digital transmitter solutions.

RF transmitter	
Hardware complexity and power consumption	
<b>Conventional solution (pico BS)</b>	
Digital front-end (DUC, DPD,...)	~ 2W
DAC	~ 1W
Transmitter (RF)	~ 1W
PA	Depends on Pout and efficiency
<b>Digital transmitter solution</b>	
Digital front-end	≪ 2W (No DPD, only simple modulator pre-processing)
DAC	Not needed
Digital RF modulator	< 1W
PA	Depends on Pout and efficiency

Nevertheless, there are also some drawbacks in the proposed digital RF modulator, in particular:

- limited time-resolution;
- various distortions from the phase modulators as zero order hold, pulse swallowing, etc.

These distortions generally reduce the signal quality (e.g., error vector magnitude (EVM) performance) and increase the out-of band emissions (e.g., in terms of adjacent channel power ratio (ACPR)) which have to be considered in view of revised, possibly relaxed overall system specifications for massive MIMO systems in heterogeneous networks.

Although the modulator concept and implementation determines the best achievable RF signal quality and the minimum achievable out-of-band emission, the PA normally dominates the final performance in terms of EVM and ACPR as long as no linearization is applied. The

reason for this is that efficient PAs are operated in their highly nonlinear region. If the spectral and signal quality requirements cannot be fulfilled, linearization (e.g., digital pre-distortion (DPD)) has to be applied. In general, the complexity of the linearization can be relaxed for switched-mode PAs because ideally they just get switched on or off, and they will not operate along the nonlinear AM-AM and AM-PM curves as conventional PAs. This is an important topic in the feasibility study carried out in WP2 and must be considered closely together with system-level simulations of the massive MIMO concept, to figure out what EVM values and ACPR levels of the individual transmitters can be tolerated.

## 3.2 Definition of performance metrics

We will now define the following two main performance metrics: the SE per cell and the total energy efficiency.

The total SE in cell  $j$  is given by

$$SE_j = \sum_{k=1}^K SE_{jk} \quad [\text{bit/s/Hz/cell}], \quad (3.3)$$

which is the sum of the SEs achieved by each of the UEs in the cell (these can be computed according to Theorem 1) in Section 2.5. The total SE is  $\zeta^{(\text{ul})}SE_j$  in the UL and  $\zeta^{(\text{dl})}SE_j$  in the DL.

For an effective transmission bandwidth of  $W$  Hz, the corresponding sum rate in cell  $j$

$$R_j = W SE_j \quad [\text{bit/s/cell}], \quad (3.4)$$

where  $\zeta^{(\text{ul})}R_j$  is the sum rate in the UL and  $\zeta^{(\text{dl})}R_j$  is the sum rate in the DL.

The total energy efficiency (EE) in a cell  $j$  is the ratio between the total transmission rate (in bit/s/cell) and the total energy expenditure (in Joule/s/cell). This leads to

$$EE_j = \frac{W SE_j}{\frac{P_{\text{tx}}}{\nu} + P_{\text{Analog}_j} + P_{\text{Baseband}_j} + K P_{\text{Terminal}}} \quad [\text{bit/Joule}], \quad (3.5)$$

where  $P_{\text{tx}}$  is the average transmission power (for the UL and DL) and  $\nu$  is the corresponding power efficiency. The power of the analog front-end at the BS  $j$ ,  $P_{\text{Analog}_j}$ , was defined in (3.1) and the power of the digital baseband power,  $P_{\text{Baseband}_j}$ , was defined in (3.2). Finally, the term  $P_{\text{Terminal}}$  models the power consumption per active UE. This term is not explicitly modeled in this document, since the focus is on massive MIMO BSs.

## Chapter 4

# Performance analysis, fundamental limits, and tradeoffs

In this chapter, we illustrate the achievable SEs in a variety of different setups and how they are affected by the main scenario parameters. We consider a general multi-cellular network with hexagonal cells and an unlimited demand for service, which means that any number of UEs  $K$  can be scheduled for UL/DL transmission with any SE. Other specific scenarios are considered in Section 4.4.

These results provide fundamental limits of the massive MIMO performance. Even if some assumptions and parameter values are not always realistic, the conclusions yield a valuable first insight that will be used to steer the research on algorithm development (e.g. on channel estimation, pilot allocation, and precoding/combining) in MAMMOET WP3.

### 4.1 Asymptotic analysis

We first consider the asymptotic limits of the SE per UE, as the number of antennas grows large. When  $M \rightarrow \infty$  (with  $K, B \leq S < \infty$ ), the effective SEs from Theorem 1 in Section 2.5 with MR, ZF, and P-ZF processing converge to a finite limit:

$$\text{SE}_{jk} \rightarrow \left(1 - \frac{B}{S}\right) \log_2 \left(1 + \frac{B}{\sum_{l \in \mathcal{L}} \sum_{\substack{m=1 \\ (l,m) \neq (j,k)}}^K \mu_{jl}^{(2)} \mathbf{v}_{i_{jk}}^H \mathbf{v}_{i_{lm}}}\right). \quad (4.1)$$

The effect of pilot contamination is very clear, since only the UEs that interfered during pilot transmission (i.e.,  $\mathbf{v}_{i_{jk}}^H \mathbf{v}_{i_{lm}} \neq 0$ ) affect the asymptotic limit. In order to maximize the asymptotic SINR in (4.1), we should allocate the pilot signals such that  $\mathbf{v}_{i_{jk}}^H \mathbf{v}_{i_{lm}} = 0$  whenever  $\mu_{jl}^{(2)}$  is large. If  $\beta = \frac{B}{K}$  is an integer, this amounts to allocating orthogonal pilots among the UEs in each cell and making sure that only  $\frac{1}{\beta}$  of the interfering cells reuse these pilots. We refer to this as *fractional pilot reuse* and let  $\beta$  denote the *pilot reuse factor*. An explicit example is provided in the next section for hexagonal cells.

For any network topology, let  $B = K\beta$  for some integer  $\beta$  and assume orthogonal pilot signals within each cell. Let  $\mathcal{L}_j \subset \mathcal{L}$  be the set of cells that use the same pilots as cell  $j$ . The

SE in cell  $j$  approaches

$$SE_j^\infty = K \left(1 - \frac{K\beta}{S}\right) \log_2 \left(1 + \frac{1}{\sum_{l \in \mathcal{L}_j \setminus \{j\}} \mu_{jl}^{(2)}}\right), \quad (4.2)$$

when  $M \rightarrow \infty$ . This SE is maximized jointly for all cells when the number of scheduled UEs is either  $K^* = \lfloor \frac{S}{2\beta} \rfloor$  or  $K^* = \lceil \frac{S}{2\beta} \rceil$  (i.e., one of the closest integers to  $\frac{S}{2\beta}$ ).

This means that the number of scheduled UEs should be proportional to the frame length  $S$  (when  $M$  is large enough); for example, we get  $K^* = \frac{S}{2}$  for  $\beta = 1$  and  $K^* = \frac{S}{6}$  for  $\beta = 3$ . Since both  $S = 200$  and  $S = 10000$  are reasonable coherence block lengths in practice, depending on the UE mobility and propagation environment, this means that we should schedule between tens and several thousands of UEs for simultaneous transmission in order to be optimal (assuming infinite demand). This is only possible if the UE selection policy is scalable and there is a high load of UEs. If  $K^* = \frac{S}{2\beta}$  is an integer, the asymptotically optimal SE is

$$SE_j^\infty = \frac{S}{4\beta} \log_2 \left(1 + \frac{1}{\sum_{l \in \mathcal{L}_j \setminus \{j\}} \mu_{jl}^{(2)}}\right) \quad (4.3)$$

and increases linearly with  $S$  (in the large- $M$  regime).

Interestingly, the optimal scheduling when  $M$  is large gives  $B = \frac{S}{2}$  for any  $\beta$ , which means that *half* the frame is used for pilot transmission.

## 4.2 Optimizing performance in hexagonal networks

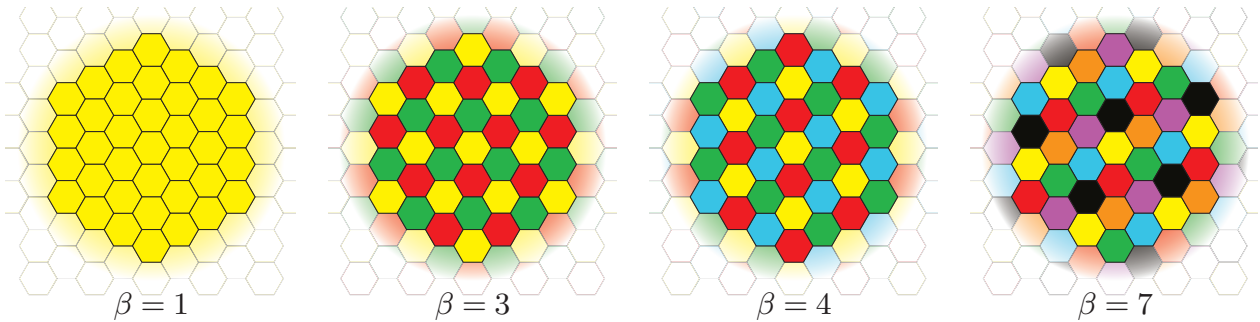
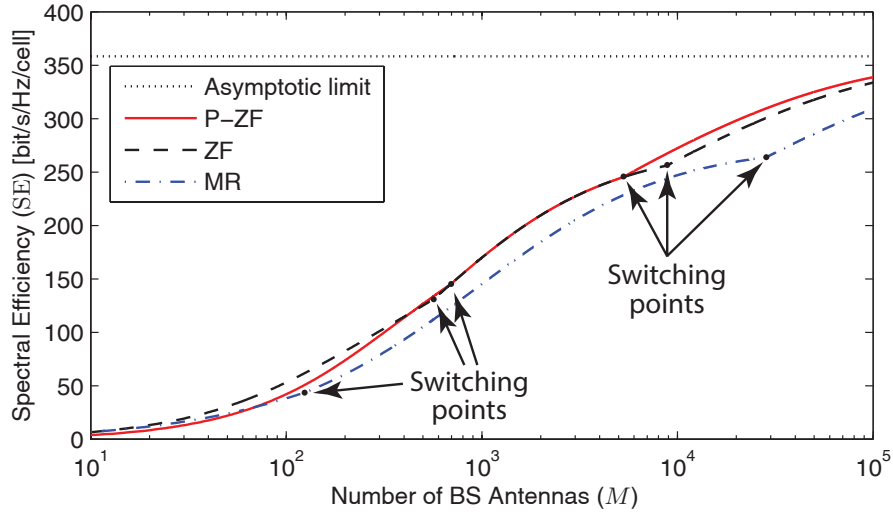


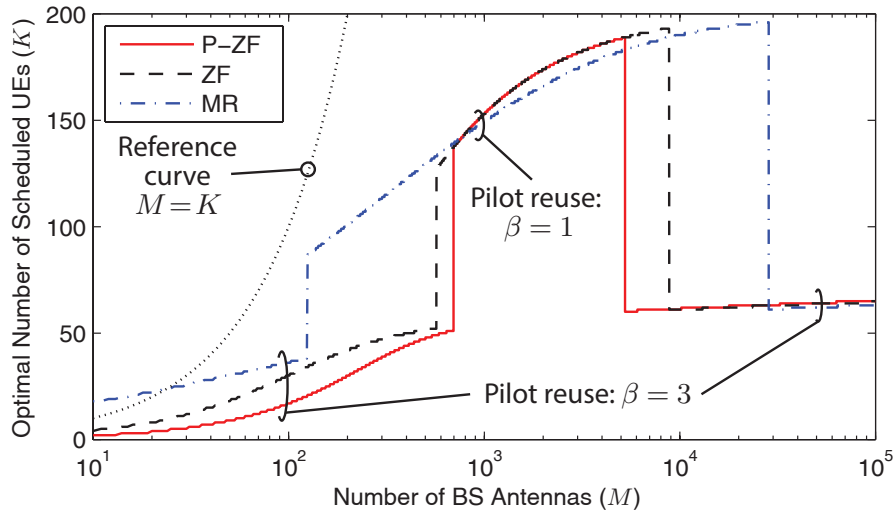
Figure 4.1: Part of a hexagonal network, colored for different pilot reuse factors  $\beta$ .

In this section, we consider the symmetric network topology depicted in Figure 4.1 with hexagonal cells. All the time/frequency resources allocated for payload data transmission are used in all cells. However, we consider pilot books of size  $B = \beta K$  to allow for fractional pilot reuse that mitigates pilot contamination from neighboring cells. The hexagonal grid is infinitely large, to avoid edge effect and giving all cells the same properties. The cell radius is defined as  $r > 0$ , which is the distance from the center to the corners. By the hexagonal structure, only  $\beta \in \{1, 3, 4, 7, \dots\}$  leads to symmetric pilot reuse patterns [21, 26] and will thus be the only pilot reuse factors considered in the simulations. The simulations consider a classic pathloss model where the variance of the channel attenuation in (2.1) is  $d_j(\mathbf{z}) = \frac{C}{\|\mathbf{z} - \mathbf{b}_j\|^\kappa}$ , where  $\|\cdot\|$  is the Euclidean norm,  $C > 0$  is a reference value, and  $\kappa \geq 2$  is the pathloss exponent. These assumptions allow us to compute  $\mu_{jl}^{(\gamma)}$  in (2.19) as

$$\mu_{jl}^{(\gamma)} = \mathbb{E}_{\mathbf{z}_{lm}} \left\{ \left( \frac{d_j(\mathbf{z}_{lm})}{d_l(\mathbf{z}_{lm})} \right)^\gamma \right\} = \mathbb{E}_{\mathbf{z}_{lm}} \left\{ \left( \frac{\|\mathbf{z}_{lm} - \mathbf{b}_l\|}{\|\mathbf{z}_{lm} - \mathbf{b}_j\|} \right)^{\kappa\gamma} \right\} \quad (4.4)$$



(a) Optimized SE per cell.

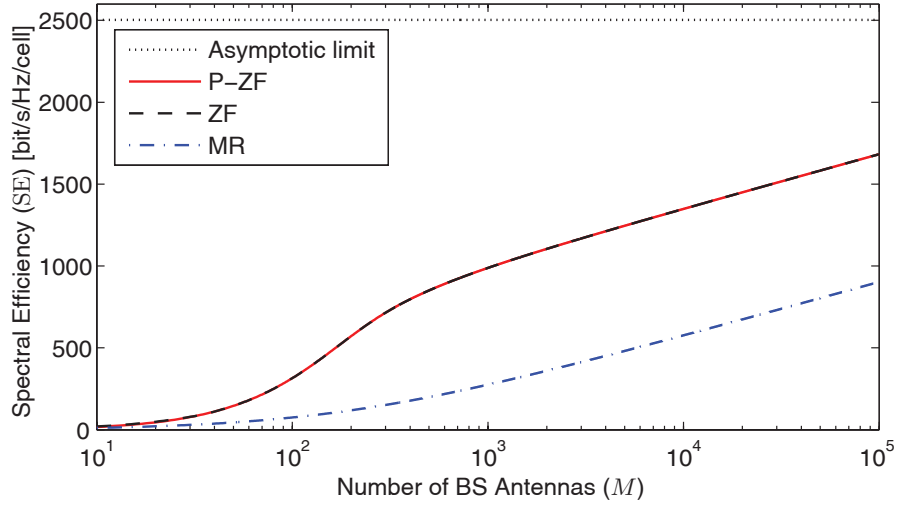
(b) Corresponding optimal number of UEs:  $K^*$ .Figure 4.2: Simulation of optimized SE, as a function of  $M$ , with average inter-cell interference.

for any UE distribution in the cells. We notice that  $C$  and  $r$  cancel out in (4.4), if the UE distribution is invariant to the radius. Since the SE per UE in Theorem 1 in Section 2.5 is independent of the UE's position, we only need to define the parameter ratio  $\rho/\sigma^2$ ; that is, the average SNR (over fading) between any UE and any antenna at its serving BS.

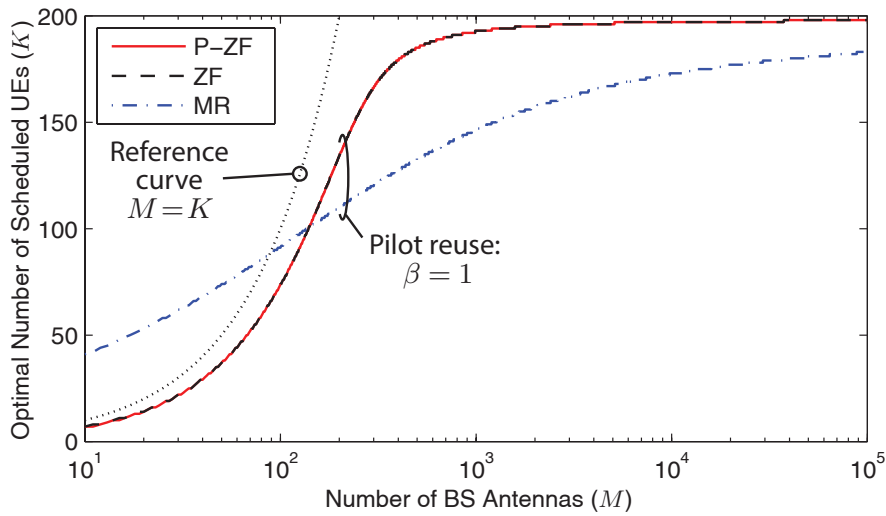
#### 4.2.1 Optimizing spectral efficiency for different interference levels

We simulate the SE in an arbitrary cell on the hexagonal grid in Figure 4.1 and take all non-negligible interference into account. Since the SE expression in Theorem 1 is the same for the UL and DL, except for the fractions  $\zeta^{(ul)}$  and  $\zeta^{(dl)}$ , we simulate the sum of these SEs and note that it can be divided arbitrarily between the UL and DL. The same linear processing schemes are used in both directions. The simulations consider MR, ZF, and P-ZF precoding/combining.

For each number of antennas,  $M$ , we optimize the SE with respect to the number of UEs  $K$  and the pilot reuse factor  $\beta$  (which jointly determine  $B = \beta K$ ). We set the coherence block length to  $S = 400$  (e.g., achieved by 2 ms coherence time and 200 kHz coherence bandwidth), pick  $\kappa = 3.7$  as pathloss exponent, and set the SNR to 5 dB. These numbers are varied in



(a) Optimized SE per cell.

(b) Corresponding optimal number of UEs:  $K^*$ .Figure 4.3: Simulation of optimized SE, as a function of  $M$ , with best-case inter-cell interference.

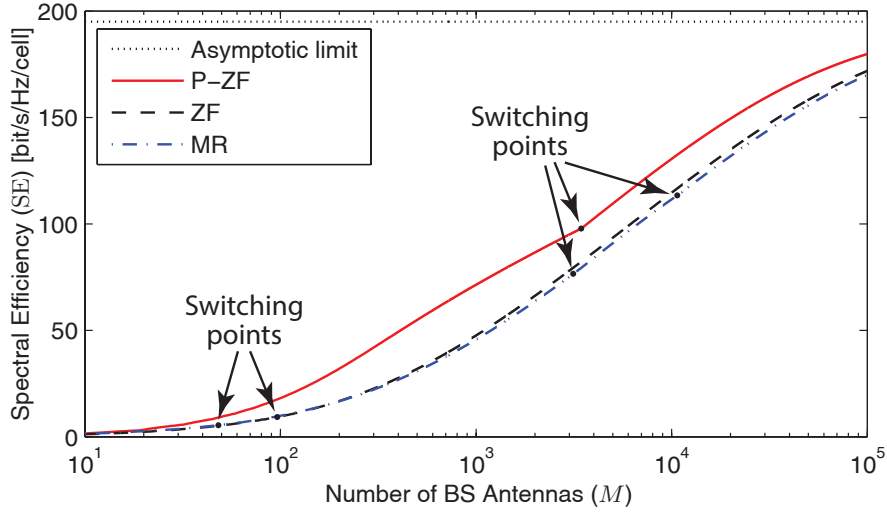
## Section 4.2.2.

We consider three propagation environments with different severity of inter-cell interference:

1. Average case: Averaging over uniform UE locations in all cells (restricting all UEs to be at least  $0.14r$  from the serving BS);
2. Best case: All UEs in other cells are at the cell edge furthest from BS  $j$  (for each  $j$ ).
3. Worst case: All UEs in other cells are at the cell edge closest to BS  $j$  (for each  $j$ ).

The corresponding values on the parameters  $\mu_{jl}^{(1)}$  and  $\mu_{jl}^{(2)}$  were computed by Monte-Carlo simulations with  $10^6$  UE locations per cell.

The best case is overly optimistic since the desirable UEs position in the interfering cells is different with respect to different cells. However, it gives an upper bound on what is achievable by coordinated scheduling across cells. The worst case is overly pessimistic since the UEs cannot all be at the worst locations with respect to all other cells, at the same time. The average case is probably the most applicable in practical deployments, where the averaging comes from both



(a) Optimized SE per cell.

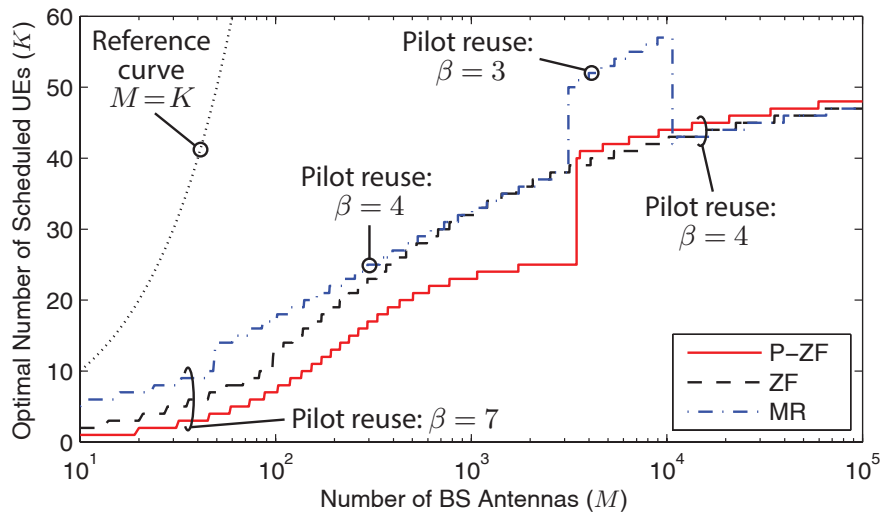
(b) Corresponding optimal number of UEs:  $K^*$ .

Figure 4.4: Simulation of optimized SE, as a function of  $M$ , with worst-case inter-cell interference.

UE mobility and (pseudo-)random switching of pilot sequences between the UEs in each cell. Results for the average case are shown in Figure 4.2, the best case in Figure 4.3, and the worst case in Figure 4.4. The optimized SE and the corresponding  $K^*$  are shown in (a) and (b), respectively.

The achievable SEs (per cell) are very different between the best case interference and the two other cases—this confirms the fact that single-cell analysis of massive MIMO is often not applicable to multi-cell cases (and vice versa). ZF brings much higher SEs than MR under the best case inter-cell interference, since then the potential gain from mitigating intra-cell interference is very high. P-ZF is equivalent to ZF in the best case, but also excels under worst case inter-cell interference since it can actively suppress also inter-cell interference. In the realistic average case, the optimized SEs are rather similar for MR, ZF, and P-ZF; particularly in the practical range of  $10 \leq M \leq 200$  antennas. In all cases, the largest differences appear when the number of antennas is very large (notice the logarithmic  $M$ -scales). At least  $M = 10^5$  antennas are needed to come close to the asymptotic limit in (4.3), and many more antennas are required under best case interference. Clearly, the asymptotic limits should generally not be

used as performance indicators since unrealistically many antennas are needed for convergence.

As seen from Figures 4.2–4.4, the main difference between MR, ZF, and P-ZF is not the values of the optimized SE but how they are achieved; that is, which number of UEs  $K^*$  and which pilot reuse factor  $\beta$  that are used. The general behavior is that larger  $M$  implies a higher  $K^*$  and a smaller  $\beta$ . Since the reuse factor is an integer,  $K^*$  changes non-continuously when  $\beta$  is changed; smaller  $\beta$  allows for larger  $K^*$ , and vice versa. MR usually schedules the largest number of UEs and switches to a smaller reuse factor at a smaller number of antennas than the other schemes. In contrast, P-ZF schedules the smallest number of UEs and has the highest preference of large reuse factors, since this it can suppress more inter-cell interference in these cases. Simply speaking, MR gives low per-user SEs to many UEs (sometimes more than  $M$ ), while ZF and P-ZF give higher per-user SEs to fewer UEs.

Recall that  $K = \frac{S}{2\beta}$  becomes the optimal number of UEs as  $M$  grows, irrespective of the processing scheme. This property is confirmed by Figures 4.2–4.4, since  $K^* \rightarrow 67$  in the average case (where  $\beta = 3$ ),  $K^* \rightarrow 200$  in the best case (where  $\beta = 1$ ), and  $K^* \rightarrow 50$  in the worst case (where  $\beta = 4$ ).

## 4.2.2 Impact of scenario parameters

We now focus on the average case of inter-cell interference, due to its practical relevance, and investigate how each scenario parameter affects the performance results. We focus on the range  $10 \leq M \leq 1000$  antennas, and when other scenario parameters than  $M$  are varied we only consider  $M = 100$  (medium massive MIMO setup) and  $M = 500$  (large massive MIMO setup).

We begin by studying the impact of the pilot reuse factor  $\beta$ . Figure 4.5 shows the per-cell SE for  $\beta = 1$  and  $\beta = 3$ , which are the ones that provide the highest SEs for  $M \leq 1000$ . The curves are smooth and there are wide regions around the  $\beta$ -switching points where both  $\beta$  values provide almost equal SEs. This robustness is positive for cell planning.

Changes in the pilot reuse factor have major impact on the optimal number of UEs and their achievable performance. The SE per UE is shown in Figure 4.6 for the operating points that maximize the SE in the cell; this is basically the ratio  $SE/K^*$  where SE was given in Figure 4.2(a) and  $K^*$  was given in Figure 4.2(b). We notice that MR gives the lowest SE per scheduled UE, while P-ZF gives the highest SE per scheduled UE. The numbers are around 1 bit/s/Hz for MR, in the range 1–2.5 bit/s/Hz for ZF, and in the range 1–3 bit/s/Hz for P-ZF. Since the pilot signaling consumes between 2 and 40 percent of the frame in this simulation, the payload data need to be encoded with up to 4.5 bit/symbol, which can be achieved by conventional 64-QAM with a 3/4 coding rate. Hence, all the per-user SEs in Figure 4.6 are straightforward to implement.

Figure 4.7 shows the ratio  $M/K^*$  for the same scenario as in the previous figures. This ratio can be interpreted as the number of BS antennas per UE [32]. There is a common rule of thumb that massive MIMO systems should have an order of magnitude more BS antennas than UEs. The operating points that satisfy this guideline are above the horizontal dotted line. This simulation indicates that an optimized system might not follow this guideline; in fact, there are a few occasions where MR even prefers to have  $M/K^* < 1$ . Generally speaking, it seems that having 2–8 BS antennas per UE is the range to aim at for practical deployments.

Since the cells might not be fully loaded at every time instant, Figure 4.8 shows the per-cell SE as a function of the number of scheduled UEs. As noted before, the peak numbers (which are star marked) are at different  $K$  for each scheme. If MR, ZF, and P-ZF are compared for a given  $K$ , the differences between the schemes can either be larger or smaller than when comparing the peak numbers. Although ZF and P-ZF often provide better SE than MR, it is interesting to

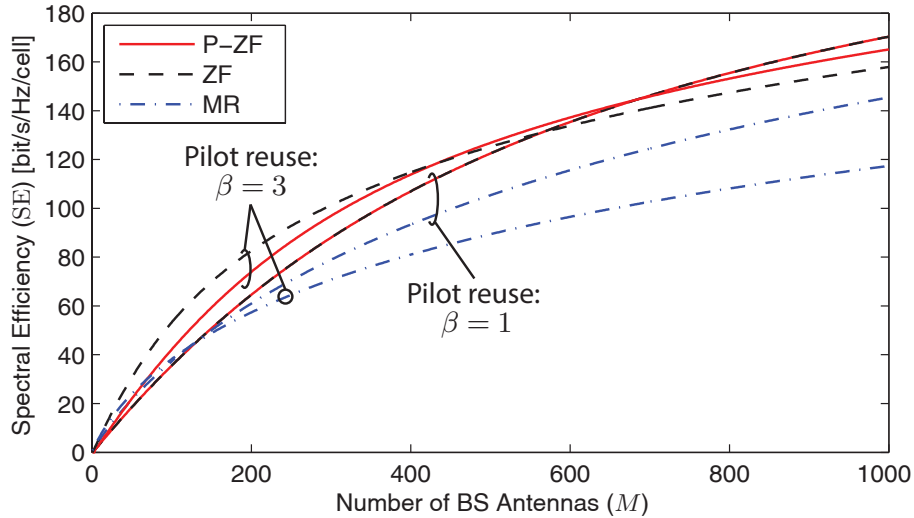


Figure 4.5: Impact of changing the pilot reuse factor  $\beta$ , for a system optimized for high per-cell SE.

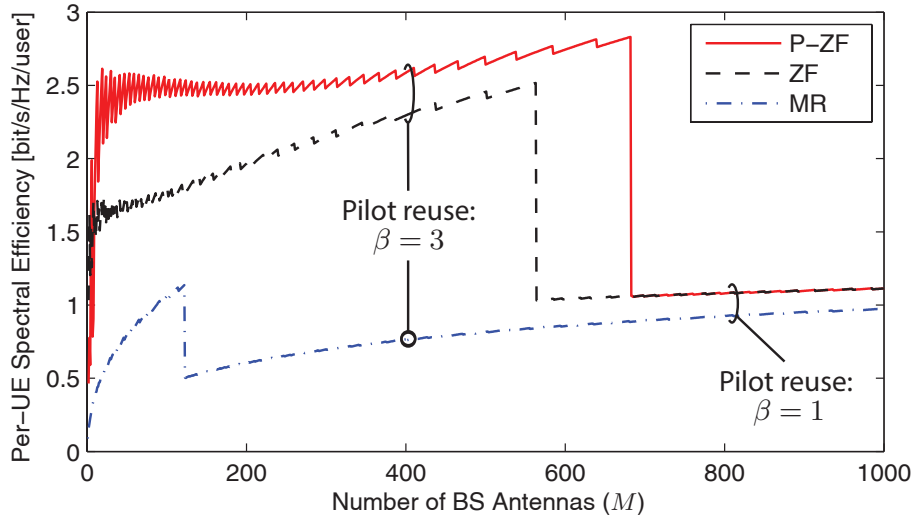


Figure 4.6: Achievable SE per UE, for a system optimized for high per-cell SE.

note that MR is competitive when  $K$  is large—both in terms of SE and since its computational complexity scales as  $\mathcal{O}(MK)$ , while the complexity of ZF and P-ZF scales as  $\mathcal{O}(MK^2)$  [15].

Next, Figure 4.9 investigates how the average SNR  $\rho/\sigma^2$  affects the results. The SE saturates already at an SNR of 5 dB due to the array gain from coherent processing—this is why that number was used in the previous figures. Massive MIMO can operate also at lower SNRs, but with a performance loss. ZF and P-ZF are particularly sensitive to the SNR level, since the active interference suppression requires a higher CSI estimation quality than simple MR processing.

The pathloss exponent  $\kappa$  determines how quickly the signals attenuate with distance. As seen from Figure 4.10, a higher pathloss exponent is beneficial in multi-cell systems since it reduces the inter-cell interference. However, this comes at the cost of spending more transmit power to achieve the target SNR of 5 dB, which is not seen in the figure.

Finally, Figure 4.11 investigates how the length of the coherence block,  $S$ , affects the per-cell SE. In the case of  $M = 100$  antennas, the gain of increasing  $S$  above 500 is relatively small—the system cannot schedule more UEs since the ratio  $M/K$  would then be too small, so the gain

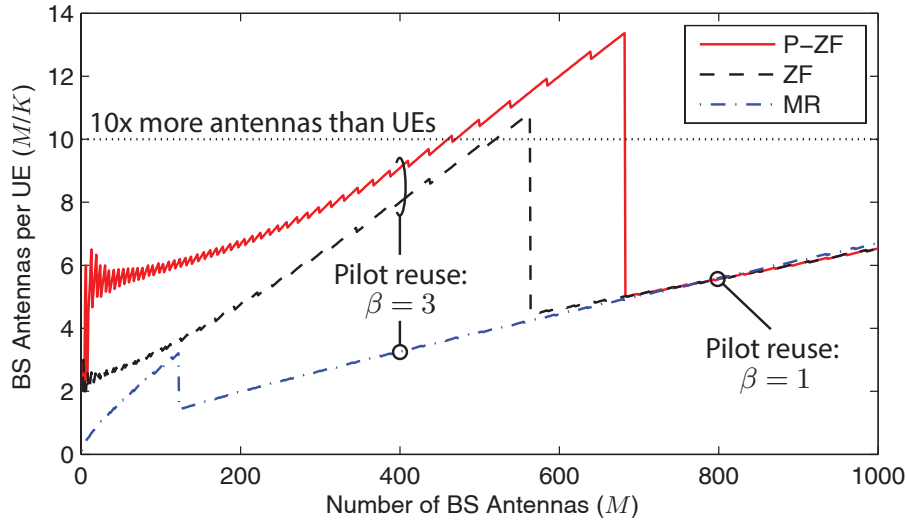


Figure 4.7: Number of BS antennas per UE, for a system optimized for high per-cell SE.

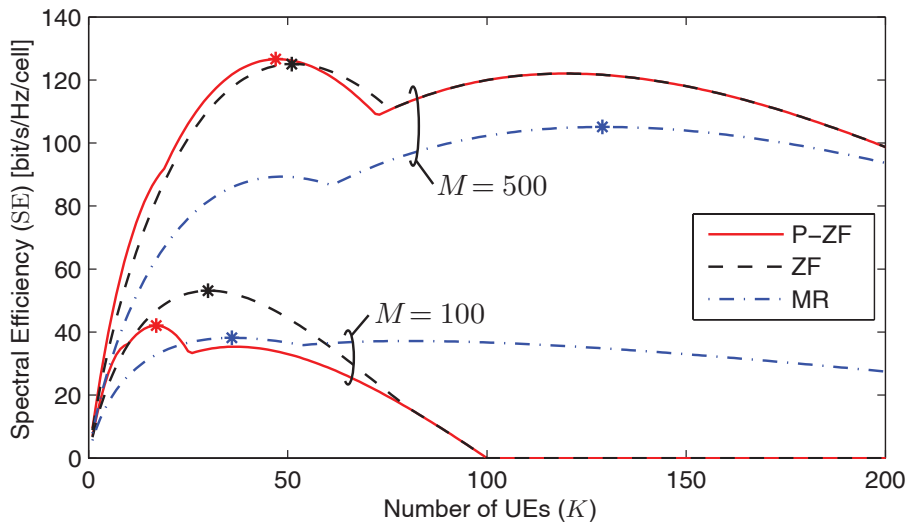


Figure 4.8: Achievable per-cell SE as a function of the number of scheduled UEs.

mainly comes from reducing the prelog factor  $(1 - \frac{B}{S})$ . However, in the case of  $M = 500$ , the system can utilize an increasing  $S$  to schedule more UEs and achieve major improvements in SE. As the number of UEs increases, the part of the intra-cell interference that cannot be rejected due to imperfect CSI becomes the main limiting factor. The benefit of P-ZF then diminishes.

### 4.3 Impact of hardware impairments

The analytic and numeric analysis in the previous sections have focused on cellular networks where the BSs and UEs are equipped with ideal transceiver hardware, which can radiate any waveform without distortions and which can receive any waveform with infinite resolution. However, any practical implementation of massive MIMO will suffer from hardware impairments, since practical transceivers inevitably operate with non-linearities in amplifiers, clock drifts in local oscillators, finite-precision ADCs, IQ imbalances, and finite-order analog filters [10, 16, 42, 51, 54].

Robustness to hardware imperfections is a very desirable feature of massive MIMO, since

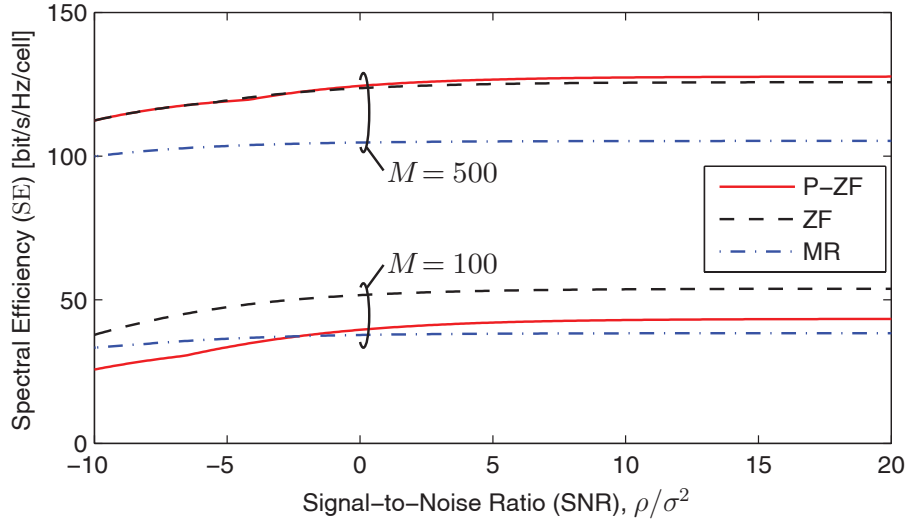


Figure 4.9: Impact of SNR variations on the SE.

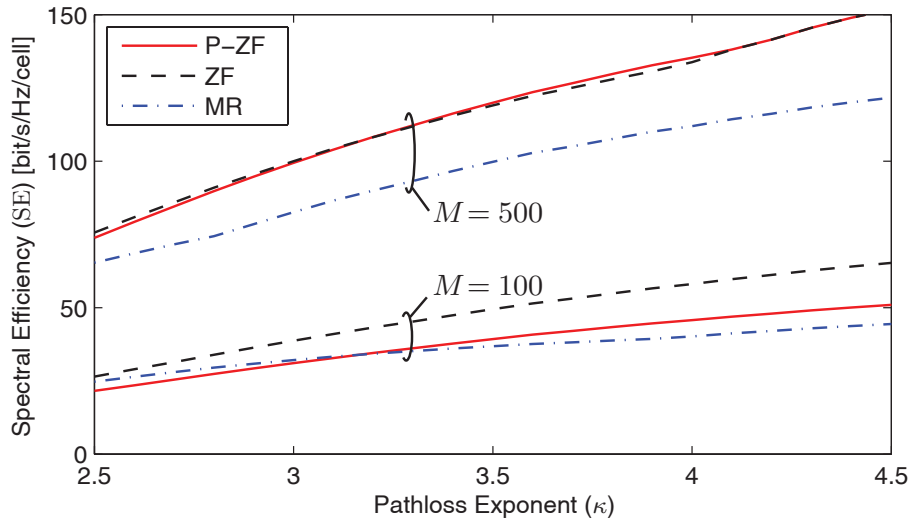


Figure 4.10: Impact of pathloss variations on the SE.

the deployment cost and circuit power consumption of massive MIMO scales linearly with the number of antennas,  $M$ , unless the hardware accuracy constraints can be relaxed—such that low-power, low-cost hardware with higher impairments are used. Fortunately, it has recently proven in [9] and [14] that massive MIMO is indeed robust to certain types of hardware impairments. More precisely, the hardware impairments in the single-antenna UEs have the same impact as in contemporary systems, while the hardware impairments at the BS array are less influential. This is, simply speaking, since the hardware impairments at each antenna can be modeled as a random additive distortion term [54]. An array gain of  $M$  is achieved when  $M$  desired signals are added coherently at the BS, while the sum of  $M$  additive distortion terms will not achieve an array gain [9]; thus, the severity of the hardware impairments in the BS array is suppressed by a factor  $M$  in massive MIMO.

This property can be utilized to gradually degrade the hardware quality as the number of antennas,  $M$ , increases. A scaling law was derived in [9], where it was shown that the variance of types of additive distortion terms can be increased proportionally to  $\sqrt{M}$ .<sup>1</sup> These design

<sup>1</sup>The reason that it cannot be increased is proportional to  $M$  is that the hardware impairments affect both

guidelines were derived for a generalized channel model, developed in [10, 16, 42, 51, 54], where the combined effect of all hardware impairments in the systems are considered, rather than the individual impairments in particular components.

These general design guidelines were confirmed in [41], where a particular hardware component was studied: namely the ADC. The analytical analysis showed that massive MIMO systems exhibit good performance even when employing 1-bit receive signal quantization. Thus, the ADC implementation complexity and power consumption can be eliminated.

In the following, we give a first-order approximation of how the hardware impairments affect the achievable SEs in massive MIMO systems, by incorporating them in the simulation setup of Section 4.2. Similar to [16, 51, 54], we model the hardware impairments as a power reduction of the original signals by a factor  $\sqrt{1 - \epsilon^2}$  and replacing it with Gaussian distortion noise that carries the removed power. The parameter  $\epsilon$  determines the level of impairments and can be interpreted as the EVM [51]; typical values in LTE are in the range  $0 \leq \epsilon \leq 0.17$  [31]. Furthermore, in MAMMOET, other models reflecting potential specific physical distortions may be considered. This will be important as some impairments can be estimated and corrected (for example IQ mismatch) while others cannot (for example some parts of the phase noise).

Figure 4.12 shows the per-cell SE in the average inter-cell interference. This figure shows results for ideal hardware with  $\epsilon = 0$  (as in Figure 4.2(a)) and for hardware impairments with  $\epsilon = 0.1$ , which is a large number in these contexts [31]. Interestingly, there is only a tiny difference in SE for  $M < 5000$ , mainly because the SE per UE is relatively small and thus the distortion noise is only a minor limiting factor. For higher number of antennas, the difference is substantial because of the asymptotic limits for ideal hardware in (4.1) does not hold under hardware impairments. Nevertheless, we conclude that hardware impairments seem to have small impact on practical massive MIMO systems, which have been optimized for high SE.

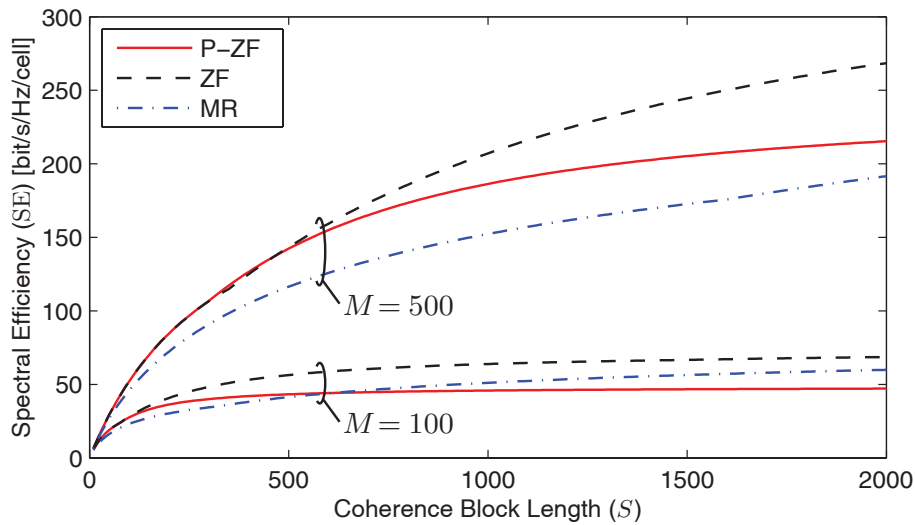


Figure 4.11: Per-cell SE as a function of the coherence block length  $S$ .

## 4.4 Specific scaling behaviors and trade-offs

In contrast to the general performance results for multi-cell systems in the previous section, this section will investigate scaling behaviors and trade-offs for certain specific setups.

the estimation and the linear processing. The combined effect of these two parts,  $\sqrt{M} \cdot \sqrt{M}$ , scales as  $M$ .

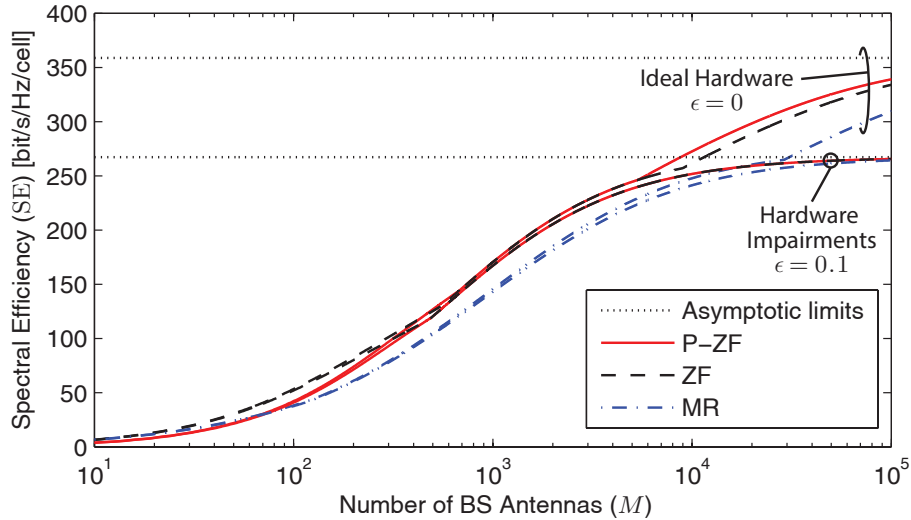


Figure 4.12: Optimized per-cell SE with or without hardware impairments.

#### 4.4.1 Energy efficiency tradeoffs

Massive MIMO systems obtain an array gain of  $M$  due to the coherent processing in the UL and DL. This array gain can be interpreted as increasing the effective SNRs by  $10 \log_{10}(M)$  dB. One way of utilizing this array gain is to reduce the transmitted power. It was shown in [9, 32, 37] that the transmit power can be reduced proportionally to  $1/\sqrt{M}$ , with only minor performance losses.<sup>2</sup> Despite the extraordinary implications of this result, the total energy efficiency metric in (3.5) is generally not maximized by this type of power reduction policy. In contrast, it was shown in [15] (using a total power model similar to the one in Section 3.1) that massive MIMO systems typically use less transmit power than conventional systems, but it should anyway be increased with  $M$ . This is explained by the fact that the power consumed by the analog front-end and digital baseband processing increases with  $M$  and thus the transmit power should be scaled accordingly to maintain a well-balanced system—that is, a system where no single component dominates the power consumption. The power of the front-end and baseband is expected to decrease over time, due to new efficient hardware generations (see Section 3.1). To maintain a well-balanced system over time, one should thus decrease also the transmit power and/or add more BS antennas [15].

Even if there might not be any drastic cuts in total transmit power in massive MIMO systems (as compared to conventional systems) in near-time, this power will be divided over a multitude of antennas. The transmit power per antenna is thus expected to decrease roughly as  $1/M$ , which means orders of magnitude less power per antenna. For example, [15] presents an EE-optimized system where the power per antenna lies in the range 10–100 mW (i.e., 10–20 dBm), while the total transmit power is around 20 dB higher. This explains why the power model in Section 3.1 assumes that the predriver provides the output for the antennas, while conventional power amplifiers might be unnecessary.

#### 4.4.2 Power allocation for realistic amplifier models

The capacity of single-user multi-antenna channels was established by E. Telatar in [45], under a sum transmit power constraint. However, this type of constraint is not realistic as it does

<sup>2</sup>The reason that the power cannot be decreased as  $1/M$  is that both the estimation and the linear processing is affected by the reduction. The combined effect of these two parts,  $1/(\sqrt{M} \cdot \sqrt{M})$ , scales as  $1/M$ .

not take into account the power dissipation in the PAs and the maximum output constraint of each individual PA.

A PA-aware model was proposed in [39], where the radiated power  $Q_n$  of the  $n$ th antenna is bounded as

$$Q_n \leq P_{\max}, \quad (4.5)$$

where  $P_{\max}$  is the maximum possible power emitted by an antenna. The consumed power  $P_{\text{cons},n}$ , which includes dissipation in the PA, is given by

$$P_{\text{cons},n} = \frac{Q_n^\varepsilon P_{\max}^{1-\varepsilon}}{\eta_{\max}}. \quad (4.6)$$

The parameter  $\eta_{\max} \in [0, 1]$  determines the power dissipation and  $\varepsilon \in [0, 1]$  determines to which extent the consumed power depends on the radiated power.

Based on this model, the MISO capacity of a frequency-flat channel was investigated in [40]. The capacity-achieving precoding was derived, for both full CSI and in the average ergodic case. In both cases, antenna selection (where only a subset of the antennas are active) is optimal for  $\varepsilon \in [0, 0.5]$ . This is because the non-linear relationship between the radiated and consumed power in (4.6) makes it beneficial to allocate either full power or no power to an antenna.

This analysis was continued in [20], where the capacity of a frequency-flat fading single-user MIMO channel was considered. The capacity-achieving solution is a linear precoder with a certain type of power allocation. Antenna selection is optimal in many situations, just as in the MISO case.

#### 4.4.3 Operation of massive MIMO in low traffic scenarios

Massive MIMO can achieve extraordinary SEs per cell, by capitalizing on the array gain and scheduling many UEs for simultaneous transmission using linear precoding/combining. The benefits of massive MIMO do not come for free, as having more antennas,  $M$ , will increase the power consumed by circuits and baseband processing at the BS. Assuming massive MIMO has been deployed in a cell, in some situations, e.g., at late night where the traffic demand is the lowest [6], having all the antennas turned on may cause a huge waste of power. Therefore one important question we are posing here is: what should the massive MIMO BSs do when the data traffic load is low?

In these cases the bulk of traffic is not likely to be delay sensitive (e.g. video streaming), therefore one can iterate between being fully turned off and sending data to everyone to meet the required data rate. In this case the most important performance metric is still the per-cell sum rate. Each individual UE can get what it desires and deserves by user scheduling. Therefore one can formulate an optimization problem with the objective to minimize the power consumed in the RF PAs (not to be confused with the radiated power), while satisfying a given performance requirement in terms of the sum rate.

This scenario was considered in [19], using the PA-aware model from (4.6), with particular focus on the DL. Figures 4.13–4.15 show the number of BS antennas in use at low SNR, moderate SNR and high SNR respectively. The results are shown against the fraction of maximum rate that the current traffic consumes. All relevant scenario parameters are found in [19]. At low SNR where users are 2.5 km away from the BS, we observe that the curves are approximately linear. For moderate and high SNR where users are 1.5 km and 1 km away from the BS respectively, the curve increases slower than linear and behaves like a convex function. One intuitive reason for this is that at low SNR, the use of excess antennas can provide an array gain to boost the sum spectral efficiency and reduce the DL transmit power. However at moderate

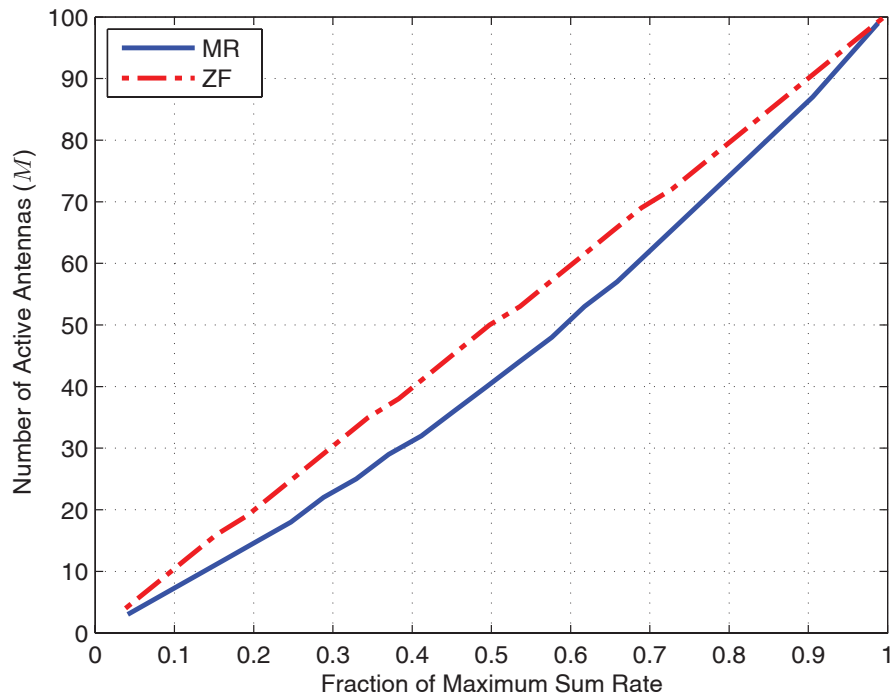


Figure 4.13: Number of BS antennas in use against fraction of maximum rate, when operating at low SNR.

and high SNR we do not need extra antennas to provide the array gain as the received power at the UE is already high enough, while using more antennas increases the power consumptions in other part of the circuits. Therefore even less antennas are needed for moderate and high SNR scenarios.

In summary, it appears that turning off BS antennas is a viable way to save energy in low traffic scenarios; the savings in circuit power consumption outweighs the loss of array gain in most cases, but there is certainly a tradeoff between these saving energy power turning of hardware and by reducing the transmit power by utilizing the array gain.

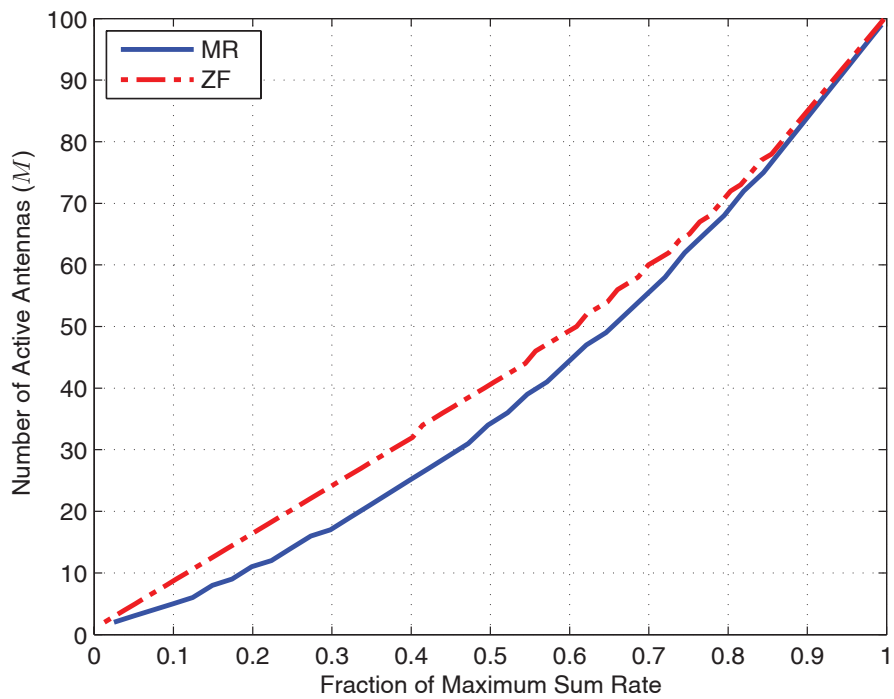


Figure 4.14: Number of BS antennas in use against fraction of maximum rate, when operating at moderate SNR.

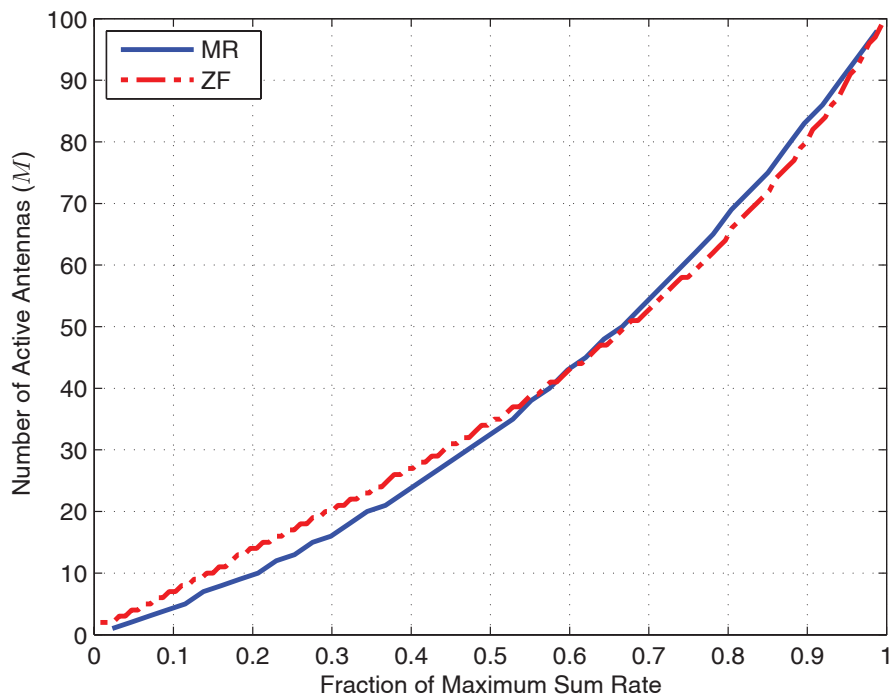


Figure 4.15: Number of BS antennas in use against fraction of maximum rate, when operating at high SNR.

## Chapter 5

# Physical layer security for massive MIMO

Even though security in massive MIMO systems is currently not in the scientific focal point, we nevertheless evaluated some of the available security approaches. The sections below report mainly a description of these approaches; however, their practical applicability in massive MIMO systems is an open research topic.

### 5.1 Background on physical layer security

People are more and more relying on the convenience of wireless technologies for the exchange of private data therefore measures have to be taken in order to secure wireless communication systems. However, due to the broadcasting nature of the wireless transmissions they lack a physical boundary. In fact, this makes them vulnerable to security breach. This mainly comes in the form of eavesdropping from unauthorised or hostile users which capture a confidential message during communication. This is the most common and easiest form of an attack on data privacy [43]. For this reason, several research organisations in various fields made efforts to elaborate profound security measures for wireless networks. One of the results of this intense investigation was a new security policy called physical layer security. The approach of physical layer security exploits properties of the physical layer of the wireless channels in order to establish secure transmission and hamper eavesdropping. Therefore, physical layer security could perfectly complement existing cryptographic techniques as it secures another stage of the communication than common cryptographic applications. In addition to this, physical layer security measures can be exploited for the generation of secret keys and their distribution.

### 5.2 Classification techniques

Physical layer security measures can be broadly classified into three different classes; namely, the power, coding, and channel methods [5].

#### 5.2.1 Power approach

This approach follows the fact that perfect secrecy is achievable when an unauthorized receiver's (eavesdropper's) channel is noisier than the legitimate receiver's channel. However, perfect secrecy can be achieved even if the channel of the eavesdropper is better than the one of

the legitimate receiver [29]. The general approach is to impose artificial noise (AN) on the unauthorized receiver's channel while the legitimate receiver's channel does not suffer from the AN [5]. In response to this, the eavesdropper receives the degraded version of the original signal due to the presence of the AN. The way of generating AN depends on how much the transmitter knows about the eavesdroppers' CSI [34]. In most cases the eavesdroppers are considered to be passive. Therefore, gaining knowledge of their CSI will not be an easy task for the transmitter. In such a case one of the most common approaches to counteract an attack is using isotropic AN design [34]. In this approach, the AN is uniformly spread on the legitimate channel's nullspace. Since the legitimate receiver does not receive the AN, it is possible for him to suppress the AN. Thus, the legitimate user can recover the original signal, whereas the eavesdropper suffers from AN [34]. In this way the transmitter can communicate with the intended receiver and prevent an attacker from eavesdropping on the message [5]. The system block diagram is shown in Figure 5.1.

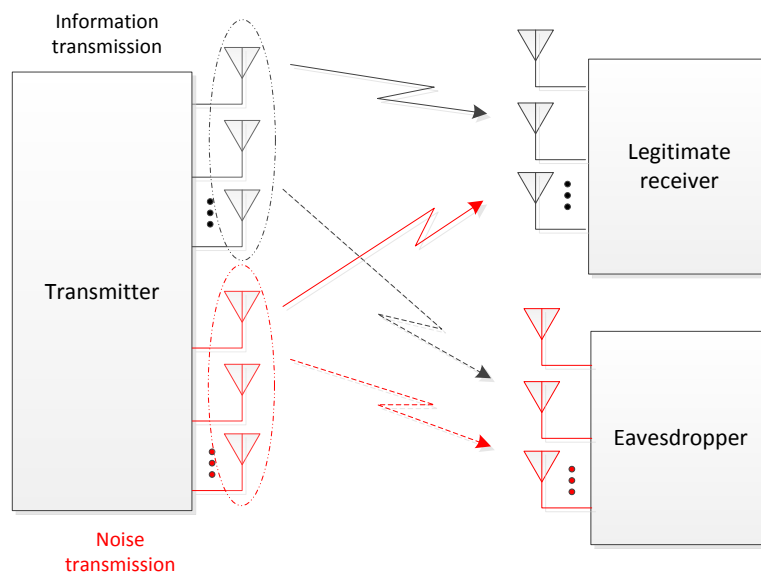


Figure 5.1: Secret communication model [50].

Another scenario could be considered if an active eavesdropper is being present. In this case, the estimation of the eavesdropper's CSI is not a major issue. With the knowledge of the eavesdropper's CSI, beamforming techniques would be much more effective. In this method, the original signal is transmitted in the direction of the legitimate user, while at the same time the AN is beamformed (matched) to the eavesdroppers' channel.

### Alternative power approach

This approach is based on a physical layer security algorithm for multiuser MIMO which makes use of a combination of the beamforming transmission and AN approach. The main idea is to split the receivers into a secure communication and interference group according to the status of each receiver's characteristics (such as SNR, security...). The interference group helps the transmitter to interfere the eavesdropper by adjusting the beamforming weights, so that it can improve the security of the secure communication group. The weights can be automatically adjusted by an interference algorithm in the transmitter or the interference group in order to force the AN into the null space of the secure communication group (in order not to affect them by AN). When the security of the receivers in the interference group is improved, they can be

switched into the secure communication group by transmitter. The system model is shown in Figure 5.2.

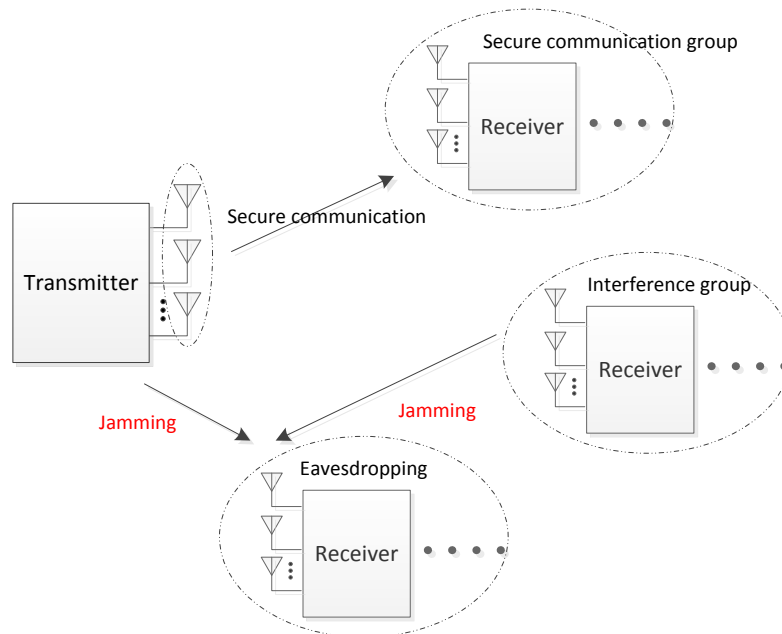


Figure 5.2: MIMO interference model [44].

The main challenge is how to split the receivers into the secure and interference group. To cope with this problem, several interference algorithm have been proposed in the literature, see e.g. [44].

### 5.2.2 Coding approach

The coding approach does not apply any special beamforming technique, which is an essential difference to the power approach described previously. However, cryptographic measures such as spread spectrum coding and error correcting codes are used to enhance the security of massive MIMO systems. In spread spectrum coding, a signal is sent on a bandwidth which is larger than the bandwidth of the original signal. This is accomplished using a pseudo random sequence in order to spread the information signal over a wider band. An advantage of this method is that the needed key could be designed much shorter than the keys for common cryptographic techniques, e.g. advanced encryption standard (AES). However, a shorter key length comes at the price of possible key-search attacks which would be more difficult when using AES [5].

In addition to encrypting the communication, error correcting codes are needed, as a slight difference between two messages leads to a distinctively different output. Therefore, errors need to be corrected before decrypting the message. There are several different error correcting codes, however, it has to be weighted which one should be used depending on the available memory and how many errors are expected to occur.

### 5.2.3 Channel approach

The channel approach makes use of the characteristics of the given channel. There are two widely used methods in order to increase the security level of MIMO systems: algebraic channel decomposition multiplexing precoding and RF fingerprinting [5].

## Algebraic channel decomposition multiplexing precoding

This approach makes use of the correlations between the single channels. Two code vectors are calculated using the singular value decomposition of the correlation matrix that corresponds to the correlation between the single channels. Then the channel between the legitimate users can be described using these code vectors. The transmitted message is then modulated using the complex code vector. However, even if an eavesdropper has all the necessary information about the code vectors, secrecy could still be achieved as the locations of the legitimate receiver and the eavesdropper differ [5].

## Radio frequency fingerprinting

This approach is based on the employment of several sensor systems to detect and identify the receivers by using the physical layer features extracted from the RF waveform of individual network packets. In response to this, the transmitter can use these identifiers to distinguish between the legitimate and illegitimate receivers within a given network. Whenever any inconsistencies are detected the communication can be disrupted or a warning can be issued. The main concern about this method is that it does not operate in real time. In order to determine the legitimate receiver, first the received signal should be stored digitally and then it should be post-processed. The post-processing consists of several computational cycles. However, further research is needed in order to realize the radio frequency fingerprint in real time [46].

## 5.3 Open issues

During the preliminary analysis reported herein, we mainly focused on the power approach as the traditional coding approach is more costly due to the need of secret key management. The feasibility analysis of the power approach methods in a massive MIMO system is the major open issue. On the one hand, the isotropic method is applicable in the presence of a passive as well as an active eavesdropper but on the other hand, it is costly in terms of complexity and power consumption. The most efficient way would be a direct beamforming method, however, as mentioned before the transmitter needs to find the location of the eavesdropper which is difficult in case of a purely passive attacker.

However, the channel approach also seems interesting for massive MIMO, so further research could be conducted on this topic.

The open issues can be formulated as follows:

- For direct beamforming of the AN to the eavesdropper's channel, the transmitter should know about the eavesdropper's CSI. The problem is how to estimate the CSI, if the eavesdropper is purely passive.
- For practical application of physical layer security methods in massive MIMO systems, the efficiency of the reported methods needs to be evaluated in order to determine which of the approaches can be implemented in practice.

# List of Abbreviations

3GPP	3rd Generation Partnership Project
5G	5th Generation
ACPR	Adjacent Channel Power Ratio
ADC	Analog-to-Digital Converter
AES	Advanced Encryption Standard
AM-AM	Amplitude-to-Amplitude Modulation
AM-PM	Amplitude-to-Phase Modulation
AN	Artificial Noise
AP	Access Point
AWGN	Additive White Gaussian Noise
BS	Base Station
BSS	Basic Service Set
BPF	Band-Pass Filter
CoMP	Coordinated Multipoint
CSI	Channel State Information
D2D	Device to Device
DAC	Digital-to-Analog Converter
DAS	Distributed Antenna System
DFE	Digital Front-End
DL	Downlink
DPD	Digital Pre-Distortion
DUC	Digital Up-Converter
EC	European Commission
EE	Energy Efficiency
EVM	Error Vector Magnitude
ESS	Extended Service Set
FDD	Frequency Division Duplex
GOPS	Giga-Operations Per Second
HEW	High Efficiency WLAN
IEEE	Institute of Electrical and Electronic Engineers

IQ	In-phase Quadrature
ITU	International Telecommunications Union
LNA	Low-Noise Amplifier
LO	Local Oscillator
LOS	Line Of Sight
LTE	Long Term Evolution
MAMMOET	Massive MIMO for Efficient Transmission
MBB	Mobile Broadband
MIMO	Multiple-Input Multiple-Output
MISO	Multiple-Input Single-Output
MCL	Minimum Coupling Losses
MMSE	Minimum Mean-Squared Error
MSE	Mean-Squared Error
MR	Maximum-Ratio
NLOS	Non Line of Sight
PA	Power Amplifier
PAPR	Peak-to-Average Power Ratio
PGA	Programmable Gain Amplifier
PWM	Pulse-width modulation
P-ZF	Pilot-based Zero-Forcing
RF	Radio Frequency
SaaS	Software as a Service
SCME	Spatial Channel Extended Model
SE	Spectral Efficiency
SG	Study Group
SINR	Signal-to-Interference-and-Noise Ratio
SNR	Signal-to-Noise Ratio
STB	Set Top Box
RF	Radio-frequency
RF-PWM	Radio-Frequency Pulse-Width Modulation
TC	Test Case
TBD	To Be Determined
TDD	Time-Division Duplex
UE	User Equipment
UL	Uplink
UMa	Urban Macro
VGA	Variable-Gain Amplifier



VoD	Video on Demand
WP	Work Package
ZF	Zero-Forcing

# Bibliography

- [1] Deliverable D1.1: Scenarios, requirements and KPIs for 5G mobile and wireless systems. Technical report, ICT-317669 METIS, April 2013.
- [2] Ericsson mobility report. Technical report, June 2014. Available: <http://www.ericsson.com/res/docs/2014/ericsson-mobility-report-june-2014.pdf>.
- [3] Deliverable D3.1: First assessment of baseband processing requirements for MaMi systems. Technical report, ICT-619086 MAMMOET, January 2015.
- [4] IEEE 802.11-13/0520r1. HEW scenarios and evaluation metrics. Technical report, May 2013.
- [5] A. Akindoyin. Physical layer security using artificial noise. Master's thesis, The University of Leeds, 2012.
- [6] G. Auer, V. Giannini, I. Godor, P. Skillermark, M. Olsson, M. A. Imran, D. Sabella, M. J. Gonzalez, C. Desset, and O. Blume. Cellular energy efficiency evaluation framework. In *Proc. IEEE VTC Spring*, 2011.
- [7] R. Baldemair, E. Dahlman, G. Fodor, G. Mildh, S. Parkvall, Y. Selen, H. Tullberg, and K. Balachandran. Evolving wireless communications: Addressing the challenges and expectations of the future. *IEEE Veh. Technol. Mag.*, 8(1):24–30, Mar. 2013.
- [8] M. Biguesh and A. B. Gershman. Downlink channel estimation in cellular systems with antenna arrays at base stations using channel probing with feedback. *EURASIP J. Appl. Signal Process.*, 2004(9):1330–1339, 2004.
- [9] E. Björnson, J. Hoydis, M. Kountouris, and M. Debbah. Massive MIMO systems with non-ideal hardware: Energy efficiency, estimation, and capacity limits. *IEEE Trans. Inf. Theory*, 60(11):7112–7139, 2014.
- [10] E. Björnson and E. Jorswieck. Optimal resource allocation in coordinated multi-cell systems. *Foundations and Trends in Communications and Information Theory*, 9(2-3):113–381, 2013.
- [11] E. Björnson, E. Jorswieck, M. Debbah, and B. Ottersten. Multi-objective signal processing optimization: The way to balance conflicting metrics in 5G systems. *IEEE Signal Process. Mag.*, 31(6):14–23, 2014.
- [12] E. Björnson, E. G. Larsson, and M. Debbah. Massive MIMO for maximal spectral efficiency: How many users and pilots should be allocated? *IEEE Trans. Wireless Commun.* Submitted, Available: <http://arxiv.org/abs/1412.7102>.

- [13] E. Björnson, E. G. Larsson, and M. Debbah. Optimizing multi-cell massive MIMO for spectral efficiency: How many users should be scheduled? In *Proc. IEEE GlobalSIP*, 2014.
- [14] E. Björnson, M. Matthaiou, and M. Debbah. Massive MIMO with non-ideal arbitrary arrays: Hardware scaling laws and circuit-aware design. *IEEE Trans. Wireless Commun.* Submitted, Available: <http://arxiv.org/abs/1409.0875>.
- [15] E. Björnson, L. Sanguinetti, J. Hoydis, and M. Debbah. Optimal design of energy-efficient multi-user MIMO systems: Is massive MIMO the answer? *IEEE Trans. Wireless Commun.* Submitted, Available: <http://arxiv.org/abs/1403.6150>.
- [16] E. Björnson, P. Zetterberg, M. Bengtsson, and B. Ottersten. Capacity limits and multiplexing gains of MIMO channels with transceiver impairments. *IEEE Commun. Lett.*, 17(1):91–94, 2013.
- [17] F. Boccardi, R.W. Heath, A. Lozano, T.L. Marzetta, and P. Popovski. Five disruptive technology directions for 5G. *IEEE Commun. Mag.*, 52(2):74–80, Feb. 2014.
- [18] H. Boche and M. Schubert. A general duality theory for uplink and downlink beamforming. In *Proc. IEEE VTC Fall*, 2002.
- [19] H. V. Cheng, D. Persson, E. Björnson, and E. G. Larsson. Massive MIMO at night: On the operation of massive MIMO in low traffic scenarios. Submitted to IEEE ICC, 2015.
- [20] H. V. Cheng, D. Persson, and E. G. Larsson. MIMO capacity under power amplifiers consumed power and per-antenna radiated power constraints. In *Proc. IEEE SPAWC*, 2014.
- [21] D. Cox. Cochannel interference considerations in frequency reuse small-coverage-area radio systems. *IEEE Trans. Commun.*, 30(1):135–142, Jan. 1982.
- [22] G. Dahman, J. Flordelis, and F. Tufvesson. On the cross-correlation properties of large-scale fading in distributed antenna systems. In *Proc. IEEE WCNC*, 2014.
- [23] C. Desset, B. Debaillie, V. Giannini, A. Fehske, G. Auer, H. Holtkamp, W. Wajda, D. Sabella, F. Richter, M. J. Gonzalez, H. Klessig, I. Gódor, M. Olsson, M. A. Imran, A. Ambrosy, and O. Blume. Flexible power modeling of LTE base stations. In *Proc. IEEE WCNC*, 2012.
- [24] C. Desset, B. Debaillie, and F. Louagie. Towards a flexible and future-proof power model for cellular base stations. In *Proc. TIWDC*, 2013.
- [25] C. Desset, B. Debaillie, and F. Louagie. Modeling the hardware power consumption of large scale antenna systems. In *Proc. IEEE OnlineGreenComm*, 2014.
- [26] V. H. Mac Donald. The cellular concept. *Bell System Technical Journal*, 58(15-41):113–381, 1979.
- [27] X. Gao, O. Edfors, F. Rusek, and F. Tufvesson. Massive MIMO in real propagation environments. *IEEE Trans. Wireless Commun.*, 2015. Accepted.
- [28] X. Gao, F. Tufvesson, and O. Edfors. Massive MIMO channels - measurements and models. In *Proc. Asilomar*, 2013.

- [29] S. Goel and R. Negi. Secret communication in presence of colluding eavesdroppers. In *Proc. IEEE MILCOM*, 2005.
- [30] K. Guo, Y. Guo, G. Fodor, and G. Ascheid. Uplink power control with MMSE receiver in multi-cell MU-massive-MIMO systems. In *Proc. IEEE ICC*, 2014.
- [31] H. Holma and A. Toskala. *LTE for UMTS: Evolution to LTE-Advanced*. Wiley, 2nd edition, 2011.
- [32] J. Hoydis, S. ten Brink, and M. Debbah. Massive MIMO in the UL/DL of cellular networks: How many antennas do we need? *IEEE J. Sel. Areas Commun.*, 31(2):160–171, Feb. 2013.
- [33] E. G. Larsson, F. Tufvesson, O. Edfors, and T. L. Marzetta. Massive MIMO for next generation wireless systems. *IEEE Commun. Mag.*, 52(2):186–195, Feb. 2014.
- [34] Q. Li and W.-K. Ma. Spatially selective artificial-noise aided transmit optimization for MISO multi-Eves secrecy rate maximization. *IEEE Trans. Signal Process.*, 61(10):2704–2717, May 2013.
- [35] T. L. Marzetta. Noncooperative cellular wireless with unlimited numbers of base station antennas. *IEEE Trans. Wireless Commun.*, 9(11):3590–3600, Nov. 2010.
- [36] R. Müller, M. Vehkaperä, and L. Cottatellucci. Blind pilot decontamination. In *Proc. ITG WSA*, 2013.
- [37] H. Q. Ngo, E. G. Larsson, and T. L. Marzetta. Energy and spectral efficiency of very large multiuser MIMO systems. *IEEE Trans. Commun.*, 61(4):1436–1449, Apr. 2013.
- [38] Nokia Siemens Networks. 2020: Beyond 4G radio evolution for the Gigabit experience. Technical report, White Paper, 2011.
- [39] D. Persson, T. Eriksson, and E. G. Larsson. Amplifier-aware multiple-input multiple-output power allocation. *IEEE Commun. Lett.*, 17(6):1112–1115, 2013.
- [40] D. Persson, T. Eriksson, and E. G. Larsson. Amplifier-aware multiple-input single-output capacity. *IEEE Trans. Commun.*, 62(3):913–919, 2014.
- [41] C. Risi, D. Persson, and E. G. Larsson. Massive MIMO with 1-bit ADC. *IEEE Trans. Commun.*, 2014. Submitted, Available: <http://arxiv.org/abs/1404.7736>.
- [42] T. Schenk. *RF Imperfections in High-Rate Wireless Systems: Impact and Digital Compensation*. Springer, 2008.
- [43] J. Sen. *Wireless Sensor Networks: Current Status and Future Trends*, chapter Security in Wireless Sensor Networks. CRC Press, 2012.
- [44] H. Song, M. Yang, X. Xu, and Wenyu Luo. A cooperative jamming based security algorithm for multi-user MIMO systems. In *Proc. IEEE ICIST*, 2013.
- [45] E. Telatar. Capacity of multi-antenna Gaussian channels. *European Trans. Telecom.*, 10(6):585–595, 1999.
- [46] A. A. Tomko, C. J. Rieser, and L. H. Buell. Physical-layer intrusion detection in wireless networks. In *Proc. IEEE MILCOM*, 2006.

- [47] 3GPP TR 36.942 V12.0.0. Radio Frequency (RF) system scenarios (release 12). Technical report, October 2014.
- [48] 3GPP TR 36.814 V9.0.0. Further advancements for E-UTRA physical layer aspects (release 9). Technical report, March 2010.
- [49] J. Vieira, F. Rusek, and F. Tufvesson. Reciprocity calibration methods for massive MIMO based on antenna coupling. In *Proc. IEEE Globecom*, 2014.
- [50] H. Wen and G. Gong. A cross-layer approach to enhance the security of wireless networks based on MIMO. In *Proc. CISS*, 2009.
- [51] M. Wenk. *MIMO-OFDM Testbed: Challenges, Implementations, and Measurement Results*. Series in microelectronics. Hartung-Gorre, 2010.
- [52] H. Yang and T.L. Marzetta. Total energy efficiency of cellular large scale antenna system multiple access mobile networks. In *Proc. IEEE OnlineGreenComm*, 2013.
- [53] H. Yin, D. Gesbert, M. Filippou, and Y. Liu. A coordinated approach to channel estimation in large-scale multiple-antenna systems. *IEEE J. Sel. Areas Commun.*, 31(2):264–273, Feb. 2013.
- [54] W. Zhang. A general framework for transmission with transceiver distortion and some applications. *IEEE Trans. Commun.*, 60(2):384–399, Feb. 2012.